DEVELOPMENT OF OXIDE NANOPHOSPHORS FOR DISPLAY APPLICATIONS

Thesis Submitted to

Delhi Technological University

in partial fulfilment of the requirements for the award of the degree of

Master of Technology
in
Nano Science & Technology

by

DILEEP KUMAR DWIVEDI
Roll No. 2k11/NST/04

Under the Joint Supervision of

Dr. M. S. MEHATA
DTU-DELHI

Dr. D. HARANATH
CSIR-NPL

DELHI TECHNOLOGICAL UNIVERSITY
NEW DELHI-110 042

JULY-2013

DECLARATION

*This is to certify that this work entitled "**Development of oxide nanophosphors for display applications**", which is submitted by me in partial fulfillment of the requirement for the completion of **M. Tech. Degree** in **Nano Science & Technology** to **Delhi Technological University (DTU) .** This dissertation comprises only my original work and it has not been published anywhere by anybody.*

(DILEEP KUMAR DWIVEDI)

In my capacity as supervisor of the candidate's thesis, I certify that the above statements are true to the best of my knowledge.

(Dr. D. HARANATH)
Thesis Supervisor
CSIR-NPL

(Dr. M. S. MEHATA)
Thesis Supervisor
DTU- DELHI

CERTIFICATE

*This is to certify that the thesis entitled "**Development of oxide nanophosphors for display applications**" is submitted in partial fulfillment of the requirements for the award of degree of **Master of Technology** in **Nano Science & Technology** at **Delhi Technological University***

*It is a faithful record of bonafide research work carried out by **Mr. Dileep Kumar Dwivedi** under my supervision and guidance. It is further certified that no part of thesis has been submitted to any other University or Institute for the award of any other Degree or Diploma to the best of my knowledge.*

Dr. D. HARANATH
Senior Scientist
Luminescent Materials and Devices Group
Material Physics Engineering Division
CSIR-National Physical Laboratory
New Delhi – 110 012

Dr. VIRENDRA SHANKER
Chief Scientist & Head
Luminescent Materials and Devices Group
Materials Physics Engineering Division
CSIR-National Physical Laboratory
New Delhi –100 012

Dr. M. S. MEHATA
Assistant Professor
Department of Applied Physics
Delhi Technological University
New Delhi – 110 042

Prof. S. C. SHARMA
Head of Department
Department of Applied Physics
Delhi Technological University
New Delhi – 110 042

ACKNOWLEDGMENTS

Any voyage in your life is incomplete without pious presence of the mercy of the One Almighty and this thesis would not have been a part of this excursion without his Grace.

"Acknowledging the good that you already have in your life is the foundation for all abundance."

I owe a sincere debt of gratitude to ***Prof. R. C. Budhani****, Director, CSIR-NPL, and* ***Prof. S.C. Sharma*** *Head of Applied Physics Department, DTU, New Delhi, for encouraging me and providing all the necessary facilities during my research work.*

I am deeply indebted to my revered research supervisor, ***Dr. D. Haranath****, Senior Scientist at Luminescent Material and Devices (LMD) group of CSIR-National Physical Laboratory, New Delhi and Project head* ***Dr. M. S. Mehata****, Assistant Professor at Applied Physics Department, DTU, New Delhi, for their inspiring guidance, thought-provoking suggestions and constant encouragement throughout my research tenure that helped me to complete this thesis in time. They taught me about all the facets of research: from experimentation to the theoretical work; very patiently and meticulously during my course of research. I express my sincere gratitude to him for everything and for introducing me to the innovative field of luminescence and nanostructures.*

My heartfelt thanks to ***Dr. Virendra Shanker****, Chief Scientist and Head, LMD Group, CSIR-NPL, whose constant inspiration, valuable suggestions and discussion at every step, improved my knowledge and helped me to complete the work in time.*

My deep regards to ***Dr. Pawan Kumar Tyagi*** *and* ***Dr. M. Jayasimhadri*** *Assistant Professors at Applied Physics Department, DTU, New Delhi, for their timely advice and support as the Course Co-ordinator and Advisor, respectively, which really helped me to carry out the project work without any obstacles.*

I should not forget to acknowledge ***Dr. Santa Chawla,*** *Principal Scientist and* ***Dr. Bipin K. Gupta****, Scientist, LMD Group, for their continuous encouragement and help in all aspects.*

It is my pleasure to acknowledge the enjoyable company, timely help and moral support rendered by ***Ms. Savvi Mishra, Mr. Amit Sharma, Ms. Deepika Yadav*** *and* ***Ms. R. Rubia*** *of LMD group. They facilitated the maintenance of a motivating working atmosphere in the group. I would like to express my gratitude to* ***Mr. Rajgir Rai****, Senior Technical Assistant of LMD group for his constant co-operation in sample preparation and for other technical assistance.*

I would like to convey my regards to ***Dr. Rajeev Chopra****,* ***Ms. Anju*** *and* ***Mr. Pushkar Joshi*** *to extend their helpful hand throughout my stay at NPL.*

I could not have reached so far in life without the blessings and wishes of my family members. Words cannot describe my deep feelings and thankfulness towards all near and dear ones. My parents – ***Mr. D .C. Dwivedi*** *and* ***Mrs. Gita Devi****; my brother* ***Mr. Pradeep Dwivedi*** *and my sister* ***Mrs. Archana Dwivedi.***

The financial assistance rendered by ***MHRD, New Delhi*** *is gratefully acknowledged.*

Place: New Delhi

Date: ***Dileep Kumar Dwivedi***

Abstract

Nanoparticles have indicated unique properties in materials, which have been different from bulk materials by a reduction in volume and an increase in the specific surface area. Properties such as band gap engineering of nanoparticles by quantum confinement and increase in reactivity due to increased specific surface area have been investigated by researchers in various fields. These materials could be utilized for light-emitting devices, fluorescent materials, catalysts and paint. Semiconductor nanoparticles are expected to have uses in bio-imaging, displays and fluorescent lights because of the controllability of both the excitation and the emission wavelengths by quantum size effects. In these applications, bio-imaging has been studied widely because of the potential realization of personalized medicine, genomic drug discovery and preventive medicine. The research of cadmium series quantum dots, which show visible fluorescence, has led to the development of a nanosize marker for bio-imaging. However, the toxicity of cadmium to the human body has been a concern.

ZnO has been one of the most promising materials for opto-electronic devices, including transparent conductive films, light emitting diodes and photocatalysts. Moreover, it has been chemically and optically stable and has a low toxicity, its use as a fluorescent label for bio-imaging has been anticipated.

It is apparent that the full potential of the as-prepared nanostructures will only be realized when materials are not only synthesized in large quantities with reproducible size, shape, structure, crystallinity, and composition but also prepared and assembled using green, environmentally friendly methodologies The sol-gel and micro-emulsion methods are versatile, practical and low cost methods for nanostructures, but they involve a final calcination or annealing step at high temperature; thus they cannot be considered to be true low-temperature synthesis methods and it is difficult to control the particle size and morphology. Hydrothermal and solvothermal syntheses are effective for synthesizing nanomaterials and available for many kinds of materials.

LIST OF ABBREVIATIONS

1. AAS - Atomic Absorption Spectroscopy
2. EDX – Energy Dispersive X-ray Analysis
3. PET-Polyethylene Terephthalate
4. EL - Electroluminescence
5. LED – Light Emitting Diode
6. OLED – Organic Light Emitting Diode
7. PDA- Personal Digital Assistant
8. PL – Photoluminescence
9. PLE - Photoluminescence Excitation
10. SEM - Scanning Electron Microscopy
11. SPS - Spark Plasma Sintering
12. TRPL- Time Resolved Photoluminescence
13. UV-VIS-NIR - Ultraviolet-Visible-Near Infra Red Spectroscopy
14. XRD - X-Ray Diffraction
15. ZGO- Zinc Gallate
16. ZSO- Zinc Silicate
17. TSL-Thermally Stimulated Luminescence

FIGURE CAPTIONS

TABLE CAPTIONS

Contents

Chapter 1

Introduction

1.1 Luminescence

There are two main processes, which cause the emission of light [1].

(a) Incandescence

This means heating an object to such a high temperature that the atoms become highly, agitated leading to the glowing of the body. The emission of this light is explained by Planck's Black Body Radiation theory. The light from the tungsten filament lamp, red-hot iron or a burning piece of coal comes under this category. Only a fraction of the total energy of the hot body appears as visible light. Most of it is dissipated as heat [2].

(b) luminescence

A cooler and more efficient mechanism of light emission is ***luminescence***. It is defined as a process whereby the matter generates a non-thermal type of optical radiation usually in the visible region of the electromagnetic spectrum. The materials that are able to convert invisible energies like UV, alpha, beta, electron, gamma, x-rays etc. into visible light are called ***luminescent materials*** or ***phosphors***. In this the light output per unit energy input is much larger than in the case of incandescence. It is because of this that for the same degree of illumination, mercury vapor based fluorescent tube lights consumes much less electricity than the household filament bulbs.

Classification of luminescence:

In luminescence, some energy source kicks an electron of an atom out of its ground or lowest energy state into an excited or higher energy state. The electron then gives back the energy in the form of light so it can fall back to its ground state. There are several varieties of luminescence, each named according to what the source of energies.

1. Photoluminescence:

This is the emission produced by excitation by the **photons**. The fluorescent lamp used in household and general lighting is the principal example of this. 254 nm UV radiations from the mercury vapor discharge are absorbed by one or more activator impurities present in the phosphor material coated on the inner side of the glass tube. Some of this energy is transferred through the process of resonance to a second impurity. By adjusting the relative concentrations of these activator impurities one can produce desired alteration in the color of the light. There are a large variety of organic and inorganic phosphors, which are used in the consumer items like in road and traffic signals, displays, laundry whiteners etc. in addition to the host of those used in industrial and scientific applications. One of the high technology called LASER is a kind of photoluminescence in which emission is coherent.

2. Electro-luminescence:

Luminescence produce by application of **electric fields** either AC or DC is called ***electro-luminescence***. There is another most popular type of electro-luminescence known is injection luminescence. In this, electrons are injected from an external supply across a semiconductor p-n junction. On applying a DC voltage across the junction, such that the electrons flow to the p- region, luminescence is produced by the electron-hole recombination in that region. The light emitting diodes (LED) which are now commonly used as display devices in many scientific instruments and gadgets are based on this principle.

3. Cathodo-luminescence:

When electron beams generated at the electrical cathodes are used for causing excitation, the emission produced is called ***cathodo-luminescence***. The screens of cathode ray tubes and television tubes glow by this kind of emission. In cathode ray tubes zinc and cadmium sulphide phosphors are used**.**

4. Radio-luminescence:

When the excitation energy is provided by x-rays or nuclear radiations, the resulting luminescence is called ***radio-luminescence***.

5. Chemi-luminescence:

Some chemical reactions are the source of luminescence. The oxidation of white phosphorous in air with extremely bright glow is the best known example of this. All chemical molecules are not capable of exhibiting luminescence.

Lyo-luminescence which is caused during the dissolution of certain compounds which have been bombarded by x-rays before-hand is also a kind of chemi-luminescence. A well-known example is the case of x-ray irradiated NaCl, which emits a flash of light when quickly, dissolved in water.

6. Bio-luminescence:

Biochemical reactions inside the cell of the living organisms can produce electronic excited states of the bio-molecules, for example, excretion of luminescent bio-molecules called ***luciferin*** in glow-worm. Fire flies, some bacteria and fungi and many sea creatures, both near surface and at great depths are the striking examples of luminescence in living beings

7. Thermo-luminescence:

The primary agent for the induction of thermo-luminescence in a material is the ionizing radiation (x-rays or gamma radiation) or sometimes even UV rays to which the material is exposed. The light produced by subsequent heating of material is called ***thermoluminescence***.

The most broadly investigated and utilized of all thermally stimulated phenomena is the emission of light during the heating of a solid sample, previously excited. The initial excitation (typically by irradiation) is the source of energy, whereas the heating serves only as a trigger which helps in releasing this accumulated energy. The term ***thermally***

stimulated luminescence (TSL) is more descriptive; however, "Thermo-luminescence" is traditionally more often utilized and popularly accepted.

Table: 1.1 Applications of various luminescence phenomena

Phenomenon	Applications
(a) Photoluminescence (PL)	Fluorescent Lamps Phototherapy Lamps Light Source Highlighting Paints and Inks Image Intensifier PLLCD PDP and other Display devices Optically pumped solid state lasers Up-conversion lasers Luminescent solar concentrators Diagnosis
(b) Radio-photoluminescence (RPL)	Dosimetry of ionizing radiations
(c) Optically stimulated luminescence (OSL)	OSL dating
(d) Radioluminescence	Watch dial, standard light source
(e) Photo-stimulated luminescence (PSL)	X-ray imaging, dosimetry
(f) Thermoluminescence (TL)	Dosimetry of ionizing radiation

	Personnel monitoring Environmental monitoring Geological dating Archaeological dating
(g) Lyoluminescence (LL)	Dosimetry of ionizing radiation Personnel monitoring
(h) Radioluminescence (Prompt)	X-ray screen X-ray scintillators Scintillation detectors
(i) Cathodoluminescence	CRO TV screens FED
(j) Electroluminescence	LED Laser diodes TFEL lamps TFEL display, TV screens
(k) Chemiluminescence	Chemical analysis

1.1.1 Photoluminescence

• Generation of excited molecules by light absorption, that then decay emitting visible light, is called *photoluminescence.*

• Physical process that leads to excited molecules can be *physical* (e.g. absorption of light), *mechanical* (e.g. friction), or *chemical* (e.g. reactions).

• When excited molecular states decay back to the ground state, resulting in the emission of light, they are undergoing a *luminescence* process.

• Molecules that have an electronic excitation are *excited.*

• Molecules that have a vibrational excitation are *hot.*

• With light absorption, molecules may become *hot* and *excited.*

• Photoluminescence processes are divided into 2 classes:

– *Fluorescence* and *Phosphorescence* based upon the duration of emission of light, the photoluminescence process could be classified as follows shown in Figure 1.1.

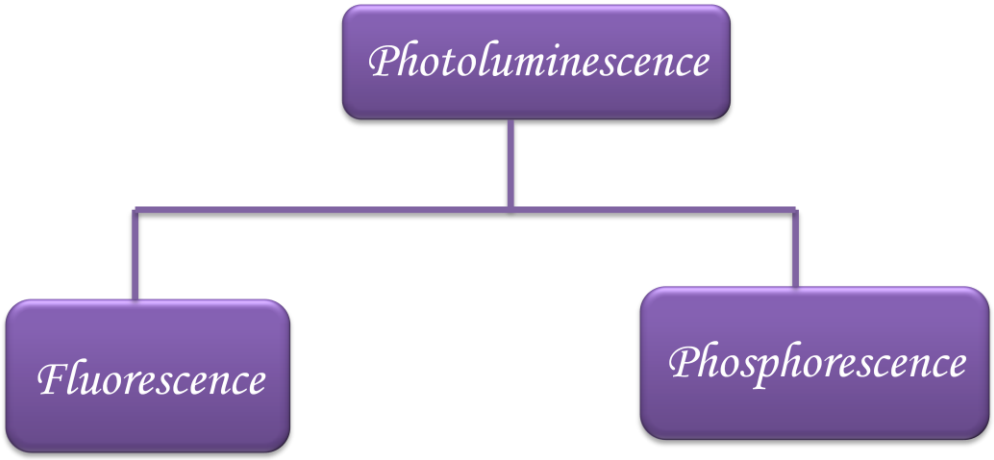

Figure 1.1: The classification of photoluminescence

Luminescence is a convenient term to cover both ***fluorescence and phosphorescence***. It is the emission of visible light from a material when excited by X-rays, ultraviolet light, electron beam, heat or friction.

Fluorescence. ($\tau \leq 10^{-7)}$ is the emission of visible light by material under the stimulus of visible or invisible radiation of shorter wavelength. If the fluorescent glow persists for an appreciable time after the stimulating rays have been cut off, this ***afterglow*** is termed as ***phosphorescence.*** Sometimes the phosphorescence may differ in color from the original fluorescence.

In brief, luminescence is defined as emission of light which is in excess of that attributable to the black body radiation and persists considerably longer than the period of the optical radiation [3].

(a) Fluorescence

• Property of some atoms or molecules to absorb light at a particular wavelength and then emit light at a longer wavelength (lower frequency) than the incident light. Absorption process occurs over short time interval ($10^{-15\ s}$) and does not change the direction of the *e* spin.

• *Vibrational relaxation* (emission of IR while lowering vibrational state) occurs in ~10^{-12s}

• De-excitation to electronic ground state with emission of lower frequency light and IR occurs in 10-9 s.

• Because vibrational relaxation occurs~1000 times faster than de-excitation, most molecules return to a low-vibrational state before the de-excitation takes place – Emitted wavelengths nearly independent of incident radiation.

• Shift in wavelength between absorption and emission spectra is the *Stokes shift*

Figure 1.2 shows the fluorescence phenomenon occurs at the time of absorption of light.

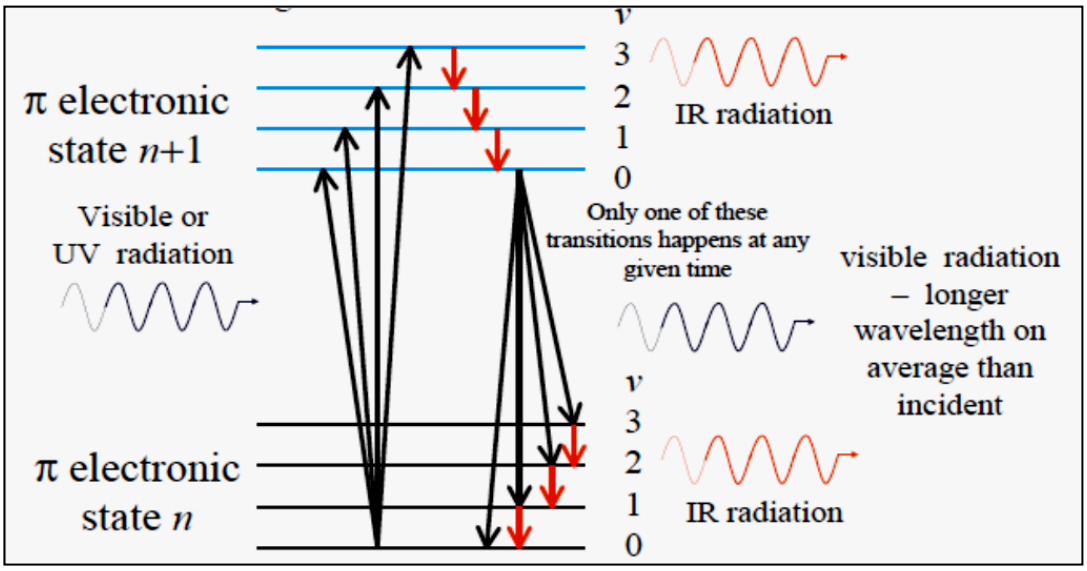

Figure 1.2: The relaxation process occur in absorption of light

(b) Phosphorescence

• In the fluorescence process, the electron did not change its spin direction but under the appropriate conditions, a spin-flip can occur.

• Spin flip can occur during absorption, or afterwards.

• The situation where no spin flip occurs, the molecule is in a *singlet state.*

• When the electron undergoes a spin-flip, a *triplet state* is created.

Figure 1.3 and 1.4 shows the phosphorescence process and change in the spin of electron when a light is absorbed.

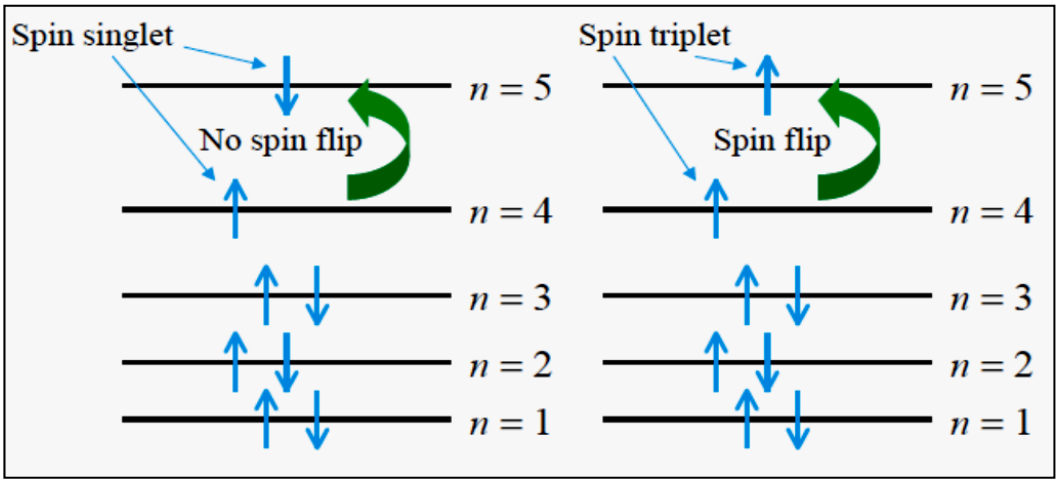

Figure 1.3: The change in the spin of a electron

• The light emission process must wait until electron undergoes a spin-flip to revert back to its original state

– May take 10-3 – 102 s

– Light emission is delayed long enough so that materials "glow in the dark" after exposure to light

– Because of the lower energy of triplet state, lower energy photon emission than incident or fluorescence photons

• Because of the long lifetimes, molecular triplet states are more often involved in photo chemical and photo-biological reactions than singlet states in molecules

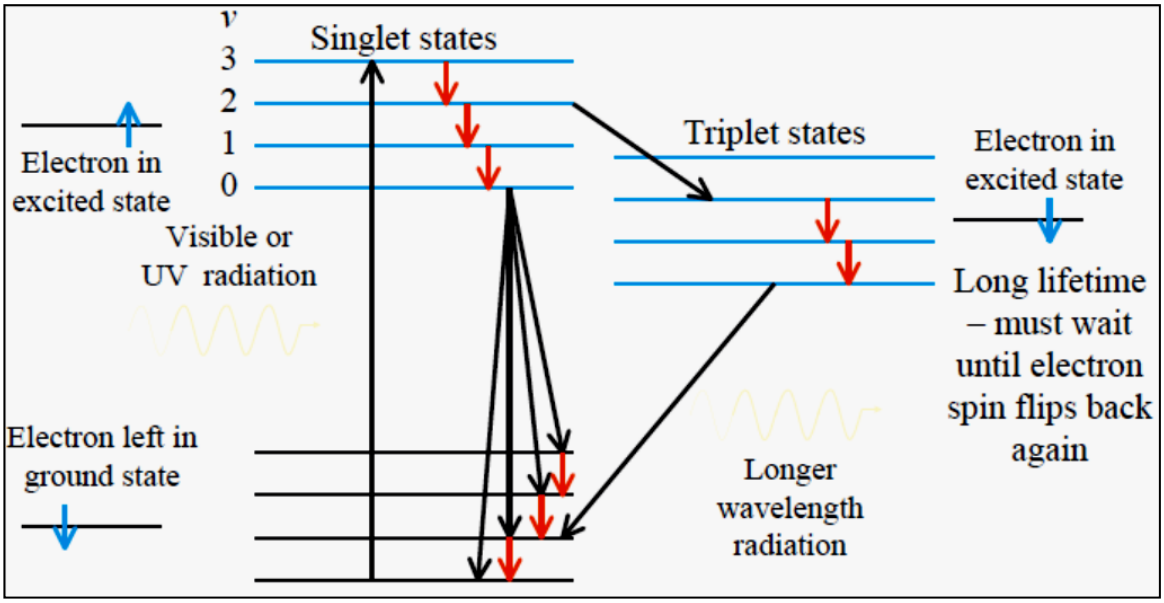

Figure 1.4: The phosphorescence process

1.2 Nanomaterials

Nanomaterials are cornerstones of nanoscience and nanotechnology. Nanostructure science and technology is a broad and interdisciplinary area of research and development activity that has been growing explosively worldwide in the past few years. It has the potential for revolutionizing the ways in which materials and products are created and the range and nature of functionalities that can be accessed. It is already having a significant commercial impact, which will assuredly increase in the future.

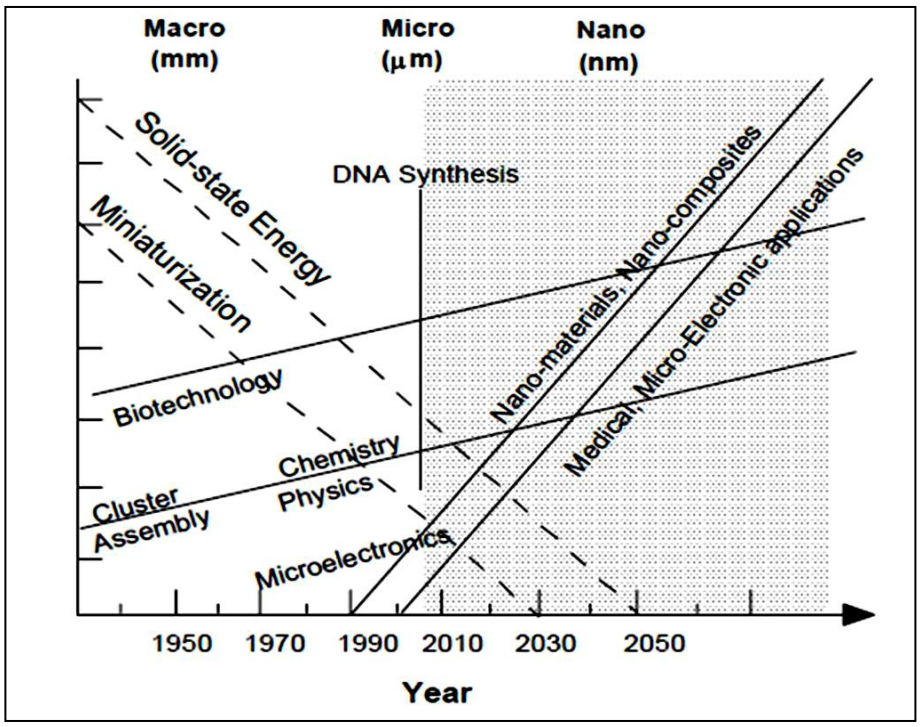

Fig. 1.5: Evolution of science and technology and the future

(a) What are nanomaterials ?

Nanoscale materials are defined as a set of substances where at least one dimension is less than approximately 100 nanometers. A nanometer is one millionth of a millimeter approximately 100,000 times smaller than the diameter of a human hair. Nanomaterials are of interest because at this scale unique optical, magnetic, electrical, and other properties

emerge. These emergent properties have the potential for great impacts in electronics, medicine, and other fields.

(b) Where are nanomaterials found ?

Some nanomaterials occur naturally, but of particular interest are engineered nanomaterials (EN), which are designed for, and already being used in many commercial products and processes. They can be found in such things as sunscreens, cosmetics, sporting goods, stain-resistant clothing, tires, electronics, as well as many other everyday items, and are used in medicine for purposes of diagnosis, imaging and drug delivery. Engineered nanomaterials are resources designed at the molecular (nanometre) level to take advantage of their small size and novel properties which are generally not seen in their conventional, bulk counterparts. The two main reasons why materials at the nanoscale can have different properties are increased relative surface area and new quantum effects. Nanomaterials have a much greater surface area to volume ratio than their conventional forms, which can lead to greater chemical reactivity and affect their strength. Also at the nanoscale, quantum effects can become much more important in determining the materials properties and characteristics, leading to novel optical, electrical and magnetic behaviours. Nanomaterials are already in commercial use, with some having been available for several years or decades. The range of commercial products available today is very broad, including stain-resistant and wrinkle-free textiles, cosmetics, sunscreens, electronics, paints and varnishes. Nanocoatings and nanocomposites are finding uses in diverse consumer products, such as windows, sports equipment, bicycles and automobiles. There are novel UV-blocking coatings on glass bottles which protect beverages from damage by sunlight, and longer-lasting tennis balls using butyl rubber nano-clay composites. Nanoscale titanium dioxide, for instance, is finding applications in cosmetics, sun-block creams and self-cleaning windows, and nanoscale silica is being used as filler in a range of products, including cosmetics and dental fillings.

1.2.1 Classification of Nanomaterials:

Nanomaterials have extremely small size which having at least one dimension 100 nm or less. Nanomaterials can be nanoscale in one dimension (eg. surface films), two dimensions (eg. strands or fibres), or three dimensions (eg. particles). They can exist in single, fused, aggregated or agglomerated forms with spherical, tubular, and irregular shapes. Common types of nanomaterials include nanotubes, dendrimers, quantum dots and fullerenes. Nanomaterials have applications in the field of nano technology, and displays different physical chemical characteristics from normal chemicals (i.e., silver nano, carbon nanotube, fullerene, photocatalyst, carbon nano, silica). According to Siegel, Nanostructured materials are classified as Zero dimensional, one dimensional, two dimensional, three dimensional nanostructures.

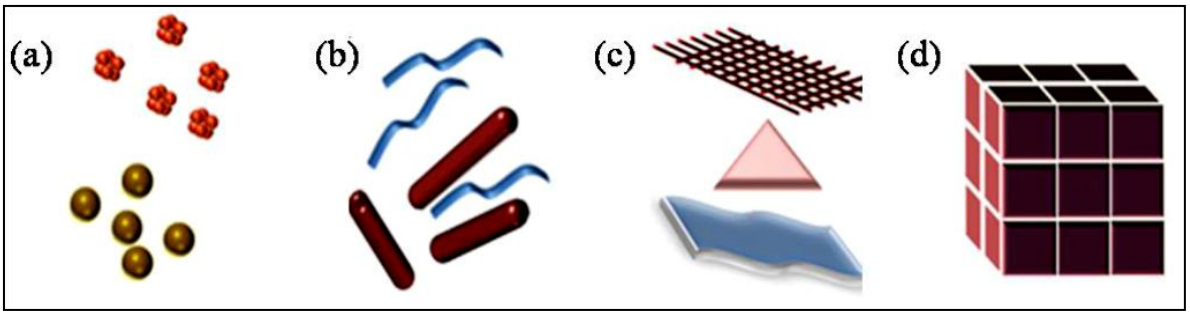

Figure 1.6 : Classification of Nanomaterials (a) 0D spheres and clusters, (b) 1D nanofibers, wires, and rods, (c) 2D films, plates, and networks, (d) 3D nanomaterials.

Nanomaterials are materials which are characterized by an ultra fine grain size (< 50 nm) or by a dimensionality limited to 50 nm. Nanomaterials can be created with various modulation dimensionalities as defined by Richard W. Siegel: zero (atomic clusters, filaments and cluster assemblies), one (multilayers), two (ultrafine-grained overlayers or buried layers), and three (nanophase materials consisting of equated nanometer sized grains) as shown in the above figure 1.6

1.2.2 Significance of nanomaterials:

These materials have created a high interest in recent years by virtue of their unusual mechanical, electrical, optical and magnetic properties. Some examples are given below:

(i) Nanophase ceramics are of particular interest because they are more ductile at elevated temperatures as compared to the coarse-grained ceramics.

(ii) Nanostructured semiconductors are known to show various non-linear optical properties. Semiconductor Q-particles also show quantum confinement effects which may lead to special properties, like the luminescence in silicon powders and silicon germanium quantum dots as infrared optoelectronic devices. Nanostructured semiconductors are used as window layers in solar cells.

(iii) Nanosized metallic powders have been used for the production of gas tight materials, dense parts and porous coatings. Cold welding properties combined with the ductility make them suitable for metal-metal bonding especially in the electronic industry.

(iv) Single nanosized magnetic particles are mono-domains and one expects that also in magnetic nanophase materials the grains correspond with domains, while boundaries on the contrary to disordered walls. Very small particles have special atomic structures with discrete electronic states, which give rise to special properties in addition to the superparamagnetism behaviour. Magnetic nanocomposites have been used for mechanical force transfer (ferrofluids), for high density information storage and magnetic refrigeration.

(v) Nanostructured metal clusters and colloids of mono- or plurimetallic composition have a special impact in catalytic applications. They may serve as precursors for new type of heterogeneous catalysts (Cortex-catalysts) and have been shown to offer substantial advantages concerning activity, selectivity and lifetime in chemical transformations and electrocatalysis (fuel cells). Enantioselective catalysis was also achieved using chiral modifiers on the surface of nanoscale metal particles.

(vi) Nanostructured metal-oxide thin films are receiving a growing attention for the realization of gas sensors (NOx, CO, CO2, CH4 and aromatic hydrocarbons) with enhanced sensitivity and selectivity. Nanostructured metal-oxide (MnO2) finds application for rechargeable batteries for cars or consumer goods. Nanocrystalline silicon films for highly transparent contacts in thin film solar cell and nano-structured titanium oxide porous films for its high transmission and significant surface area enhancement leading to strong absorption in dye sensitized solar cells.

(vii) Polymer based composites with a high content of inorganic particles leading to a high dielectric constant are interesting materials for photonic band gap structure.

1.2.3 Examples of Nanomaterials:

Nanomaterials (carbon, gold, metals, metaloxides and alloys) with variety of morphologies (shapes) are depicted in Figure 1.7.

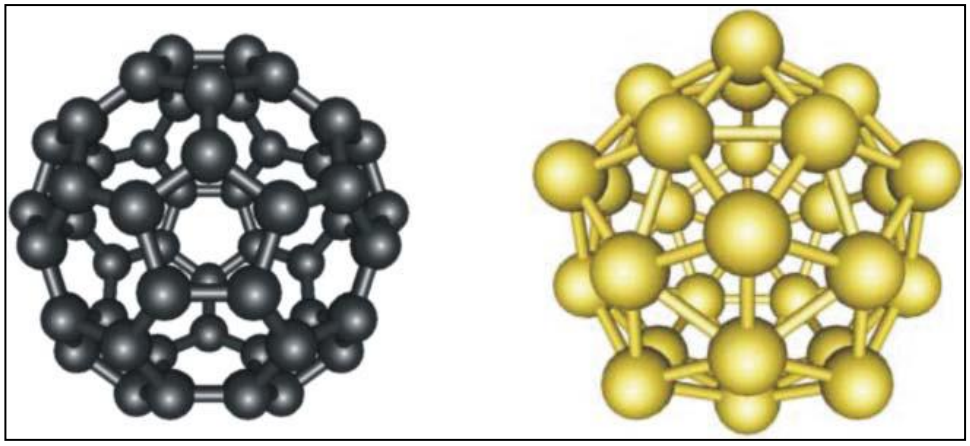

Figure1.7 Calculated structures of the fullerene C60 (left) and of the Au32 (right) nanoclusters which are both hollow.

1.3 Properties of nanomaterials:

Nanomaterials have the structural features in between of those of atoms and the bulk materials. While most microstructured materials have similar properties to the corresponding bulk materials, the properties of materials with nanometer dimensions are significantly different from those of atoms and bulks materials. This is mainly due to the nanometer size of the materials which render them: (i) large fraction of surface atoms; (ii) high surface energy; (iii) spatial confinement; (iv) reduced imperfections, which do not exist in the corresponding bulk materials.

Due to their small dimensions, nanomaterials have extremely large surface area to volume ratio, which makes a large to be the surface or interfacial atoms, resulting in more "surface" dependent material properties. Especially when the sizes of nanomaterials are comparable to length, the entire material will be affected by the surface properties of nanomaterials. This in turn may enhance or modify the properties of the bulk materials. For example, metallic nanoparticles can be used as very active catalysts. Chemical sensors from nanoparticles and nanowires enhanced the sensitivity and sensor selectivity. The nanometer feature sizes of nanomaterials also have spatial confinement effect on the materials, which bring the quantum effects.

(a) Optical properties:

One of the most fascinating and useful aspects of nanomaterials is their optical properties. Applications based on optical properties of nanomaterials include optical detector, laser, sensor, imaging, phosphor, display, solar cell, photocatalysis, photoelectrochemistry and biomedicine. The optical properties of nanomaterials depend on parameters such as feature size, shape, surface characteristics, and other variables including doping and interaction with the surrounding environment or other nanostructures. Likewise, shape can have dramatic influence on optical properties of metal nanostructures. Figure 1.8 (a) and (b) shows the variation of band gap with respect to particle size .

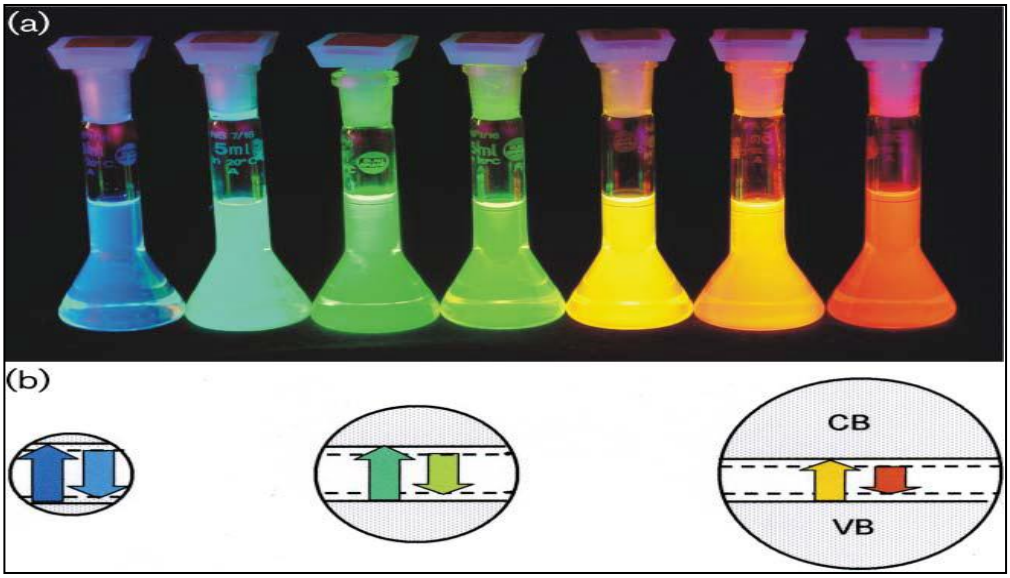

Figure1.8:(a) Fluorescence of CdSe–CdS core–shell nanoparticles with a diameter of 1.7 nm (blue) up to 6 nm (red), giving evidence of the scaling of the semiconductor band gap with particle size (b)Schematic representation of the size effect on the gap between the valence band (VB) and the conduction band (CB) and the absorption (up arrow) and fluorescence (down arrow). Smaller particles have a wider band gap.

(b) Electrical properties:

Electrical Properties of Nanoparticles" discuss about fundamentals of electrical conductivity in nanotubes and nanorods, carbon nanotubes, photoconductivity of nanorods, electrical conductivity of nanocomposites. One interesting method which can be used to demonstrate the steps in conductance is the mechanical thinning of a nanowire and measurement of the electrical current at a constant applied voltage. The important point here is that, with decreasing diameter of the wire, the number of electron wave modes contributing to the electrical conductivity is becoming increasingly smaller by well-defined quantized steps. In electrically conducting carbon nanotubes, only one electron wave mode is observed which transport the electrical current. As the lengths and orientations of the carbon nanotubes are different, they touch the surface of the mercury at different times, which provides two sets of information: (i) the influence of carbon nanotube length on the resistance; and (ii) the resistances of the different nanotubes. As the nanotubes have

different lengths, then with increasing protrusion of the fiber bundle an increasing number of carbon nanotubes will touch the surface of the mercury droplet and contribute to the electrical current transport.

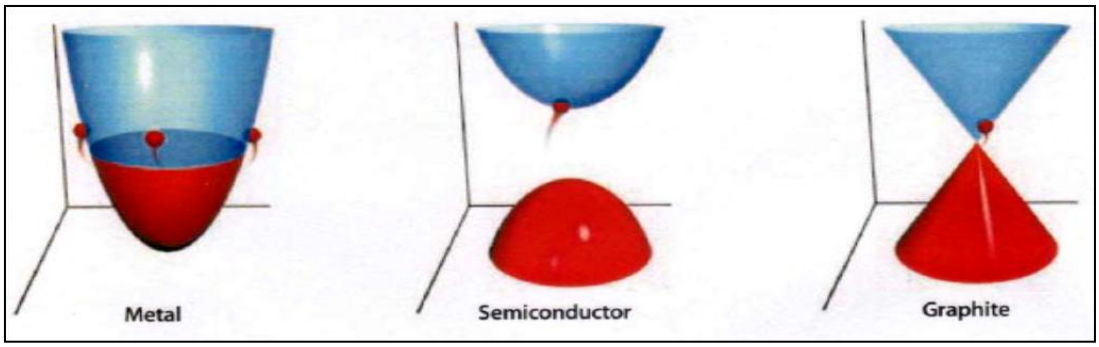

Figure 1.9 :Electrical behavior of nanotubes

(c) Mechanical properties:

"Mechanical Properties of Nanoparticles" deals with bulk metallic and ceramic materials, influence of porosity, influence of grain size, superplasticity, filled polymer composites, particle-filled polymers, polymer-based nanocomposites filled with platelets, carbon nanotube-based composites. The discussion of mechanical properties of nanomaterials is, in to some extent, only of quite basic interest, the reason being that it is problematic to produce macroscopic bodies with a high density and a grain size in the range of less than 100 nm. However, two materials, neither of which is produced by pressing and sintering, have attracted much greater interest as they will undoubtedly achieve industrial importance. These materials are polymers which contain nanoparticles or nanotubes to improve their mechanical behaviors, and severely plastic-deformed metals, which exhibit astonishing properties. However, because of their larger grain size, the latter are generally not accepted as nanomaterials. Experimental studies on the mechanical properties of bulk nanomaterials are generally impaired by major experimental problems in producing specimens with

exactly defined grain sizes and porosities. Therefore, model calculations and molecular dynamic studies are of major importance for an understanding of the mechanical properties of these materials. Filling polymers with nanoparticles or nanorods and nanotubes, respectively, leads to significant improvements in their mechanical properties. Such improvements depend heavily on the type of the filler and the way in which the filling is conducted. The latter point is of special importance, as any specific advantages of a nanoparticulate filler may be lost if the filler forms aggregates, thereby mimicking the large particles. Particulate filled polymer-based nanocomposites exhibit a broad range of failure strengths and strains. This depends on the shape of the filler, particles or platelets, and on the degree of agglomeration. In this class of material, polymers filled with silicate platelets exhibit the best mechanical properties and are of the greatest economic relevance. The larger the particles of the filler or agglomerates, the poorer are the properties obtained. Although, potentially, the best composites are those filled with nanofibers or nanotubes, experience teaches that sometimes such composites have the least ductility. On the other hand, by using carbon nanotubes it is possible to produce composite fibers with extremely high strength and strain at rupture. Among the most exciting nanocomposites are the polymer ceramic nanocomposites, where the ceramic phase is platelet-shaped. This type of composite is preferred in nature, and is found in the structure of bones, where it consists of crystallized mineral platelets of a few nanometers thickness that are bound together with collagen as the matrix. Composites consisting of a polymer matrix and defoliated phyllosilicates exhibit excellent mechanical and thermal properties.

(d) Magnetic properties:

Bulk gold and Pt are non-magnetic, but at the nano size they are magnetic. Surface atoms are not only different to bulk atoms, but they can also be modified by interaction with other chemical species, that is, by capping the nanoparticles. This phenomenon opens the possibility to modify the physical properties of the nanoparticles by capping them with appropriate molecules. Actually, it should be possible that non-ferromagnetic bulk materials exhibit ferromagnetic-like behavior when prepared in nano range. One can obtain

magnetic nanoparticles of Pd, Pt and the surprising case of Au (that is diamagnetic in bulk) from non-magnetic bulk materials. In the case of Pt and Pd, the ferromagnetism arises from the structural changes associated with size effects.

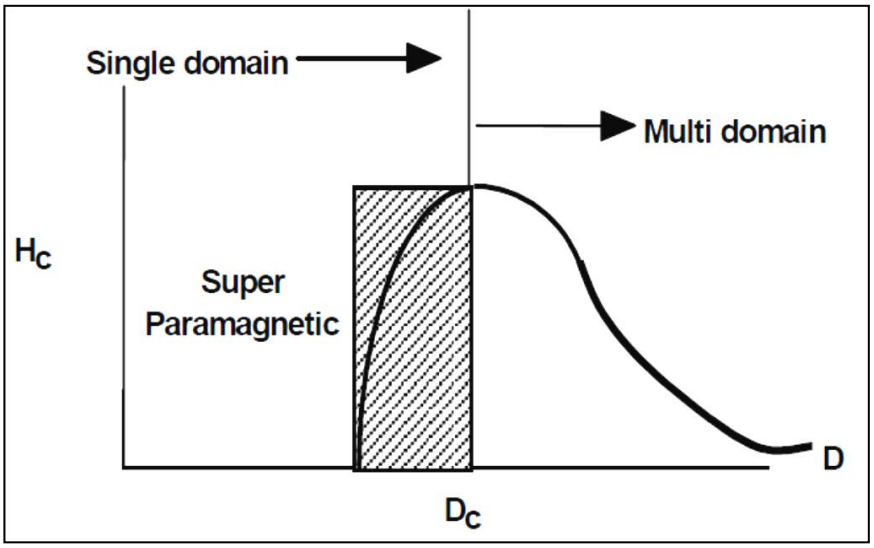

Figure 1.10: Magnetic properties of nanostrucutred materials

However, gold nanoparticles become ferromagnetic when they are capped with appropriate molecules: the charge localized at the particle surface gives rise to ferromagnetic-like behavior. Surface and the core of Au nanoparticles with 2 nm in diameter show ferromagnetic and paramagnetic character, respectively. The large spin-orbit coupling of these noble metals can yield to a large anisotropy and therefore exhibit high ordering temperatures. More surprisingly, permanent magnetism was observed up to room temperature for thiol-capped Au nanoparticles. For nanoparticles with sizes below 2 nm the localized carriers are in the 5d band. Bulk Au has an extremely low density of states and becomes diamagnetic, as is also the case for bare Au nanoparticles. This observation suggested that modification of the d band structure by chemical bonding can induce ferromagnetic like character in metallic clusters.

1.4 Literature survey

The role of nanomaterials in modern technologies is becoming increasingly significant because of the feasibility and ease of adding new functions to the existing commercial products, apart from products made completely from nanomaterials through the bulk, which is relatively difficult. Nanomaterials are usually characterized by a feature size of less than 100 nm at least in one dimension Recently in April 2010, US EPA has announced a new working definition of nanomaterials as "**an ingredient that contains particles that have been intentionally produced to have at least one dimension that measures between approximately 1 and 100 nanometers"** in order to facilitate the implementation of regulations on use of nanomaterials in commercial products The expectations on nanomaterials are enormous as their unique mechanical, optical, electrical, magnetic, thermal and catalytical properties make them special ingredients for number of applications. The market for nanotechnology over the years has not matched the initial hype that was based on the expectation that the nanotechnology based products will permeate through every industrial sector. Nevertheless, the market for nanotechnology products has grown significantly especially in the consumer products area. The successful commercialization of nanomaterials is possible only when the material production and application development proceeds in parallel with each other. Often, material production is a challenging process although it looks simple from the synthesis point of view. This is because the surface functionalities of nanoparticles have to be tailored keeping in mind the application. For example, through surface modification, a number of properties of nanoparticles like dispensability in a suspension, compactability during subsequent consolidation, colour in case of metal and semiconductor quantum dots and compatibility with the matrix material in the case of nanocomposites can be altered and often dramatically. Thus, in real practice, multiple synthesis techniques have to be evaluated for each application, leave alone for different applications. Additional challenges in large scale synthesis include consistency in product quality, cost of raw material and equipment, yield of the product, safety of the process, waste disposal and environmental issues When it comes to application development, many of the proven technologies based on

nanomaterials are related to health products, including water filters, medical textiles, cosmetics and drug delivery. Unlike USA, Europe and Japan, the Indian industries have started looking at nanotechnology only recently as a solution for their problems. Big companies like Reliance Industries, Tata Chemicals, Mahindra, Ashok Leyland, Asian Paints, Crompton Greaves have initiated programmes on nanomaterials on their own or in collaboration with academic/R&D institutions. Many of companies work on application of nanomaterials for value addition to their products but they purchase nanomaterials from abroad at high cost as the availability of nanomaterials in India is limited. Only very few institutes and industries are making efforts to develop scalable synthesis processes for mass scale production of nanomaterials. For example, International Advanced Research Centre for powder metallurgy and new materials (ARCI), an autonomous institute of DST, CSIR-NPL has taken up the responsibility of developing the synthesis processes for nanomaterials which are not only scalable for mass production but also are application specific While nanomaterial based technology development is becoming very competitive, serious attention has to be paid in the safety and toxicology issues of nanomaterial both during synthesis and application development

Definition of the Problem:

Nanomaterials are intrinsically important because their properties differ significantly from those of their bulk counterparts. Nanomaterials are widely used in various applications such as energy cells,[4-8] sensitive sensors,[9–13] nanoelectronic devices[14–21]and bio-markers[22,23]etc. Consequently, the synthesis and fabrication of functional nanomaterials with predictable, rational strategies is a key for the development of their applications. It is apparent that the full potential of the as-prepared nanostructures will only be realized when materials are not only synthesized in large quantities with reproducible size, shape, structure, crystallinity, and composition but also prepared and assembled using green, environmentally friendly methodologies. [24–27] There has been increasing interest in the development of clean synthetic procedures (green chemistry) for products targeted at

biomedical applications, surface modifications and intrinsic property investigations. An environmentally acceptable solvent system and eco-friendly reducing and capping reagents are three essential elements for a completely green synthesis. Nanocrystals have been prepared by many methods, including vapor phase process,[28,29] jet deposition,[29–31] milling,[32,33] sol-gel method,[34,35] microemulsion,[36] co-precipitation,[37] template. Although all these methods have their own advantages, most of them involve high vacuum and a high temperature, or high pressure, or a low temperature with high pressures. The categories and mass of materials prepared by the vapor phase process and jet deposition syntheses are limited, which cause the high price of the products. Although milling processes can produce large quantities of crystal powders, the diameters of the produced particles are only sub-micrometer, and the morphology of the particles is difficult to control. The sol-gel and microemulsion methods are very practical syntheses and low cost methods for nanostructures, but they involve a final syntheses,[38] hydrothermal synthesis[39–41] and solvothermal synthesis,[42,43] etc. calcination or annealing step at high temperature; thus they cannot be considered to be true low-temperature synthesis methods, and it is difficult to control the particle size and morphology. Hydrothermal and solvothermal syntheses are effective for synthesizing nanomaterials and available for many kinds of materials. However, some surfactants and capping agents used in hydrothermal or solvothermal methods are not completely removed from the final products, which can affect some of the physical properties of the crystals. In addition, large amounts of organic solvent used in solvothermal synthesis would bring about environmental pollution. Moreover, because of the high pressure involved in hydrothermal and solvothermal syntheses, sophisticated equipment is required. Various synthesis methods are reported to be capable of producing various nanostructures, but most of the methods are limited to synthesizing one type of or a specific collection of nanostructures, except a general approach is available for utilizing the hydrothermal route to synthesize a large variety of nanoparticles using fatty acids as structure-directing agents[44].

References:

[1] E. N. Harvey, A History of Luminescence; American Philosophical Society, (1957).

[2] S. Shionoya, and W. M. Yen, Phosphor Handbook; Phosphor Research Society; CRC Press: Boca Raton, FL, (1998).

[3] G. Blasse, B.C. Grabmaier, Luminescent Materials, (1994) Springer Verlag.

[4] C. F. Pan, H. Wu, C. Wang, B. Wang, L. Zhang, Z. D. Cheng, P. Hu, W. Pan, Z. Y. Zhou, X. Yang and J. Zhu, Adv. Mater., 20 (2008) 1644.

[5] U. Bach, D. Lupo, P. Comte, J. E. Moser, F. Weissortel, J. Salbeck, € H. Spreitzer and M. Gra€atzel, Nature, 395 (1998) 583.

[6] B. Tian, X. Zheng, T. J. Kempa, Y. Fang, N. Yu, G. Yu, J. Huang and C. M. Lieber, Nature 449 (2007) 885.

[7] Y. G. Guo, J. S. Hu and L. J. Wan, Adv. Mater., 20 (2008) 2878.

[8] Z. P. Shao and S. M. Haile, Nature, 431 (2004) 170.

[9] Z. H. Bao, M. R. Weatherspoon, S. Shian, Y. Cai, P. D. Graham, S. M. Allan, G. Ahmad, M. B. Dickerson, B. C. Church, Z. Kang, C. J. Summers, H. W. Abernathy, III, M. Liu and K. H. Sandhage, Nature, 446 (2007) 172.

[10] A. Serpenguzel, A. Kurt, I. Inanc € ,, J. E. Cary and E. Mazur, J. Nanophotonics, 2 (2008) 021770.

[11] J. Zhou, Y. D. Gu, P. Fei, W. J. Mai, Y. F. Gao, R. S. Yang, G. Bao and Z. L. Wang, Nano Letters, 8 (2008) 3035.

[12] L. Shang and S. J. Dong, J. Mater. Chem., 18 (2008) 4636.

[13] F. Patolsky, G. Zheng and C. M. Lieber, Anal. Chem., 78 (2006) 4260.

[14] Y. Li, F. Qian, J. Xiang and C. M. Lieber, Materials Today, 9 (2006) 18.

[15] Z. L. Wang, Adv. Func. Mater., 18 (2008) 1.

[16] M. H. Huang, S. Mao, H. Feick, H. Yan, Y. Y. Wu, H. Kind, E. Weber, R. Russo and P. Yang, Science, 292 (2001) 1897.

[17] T. Voss, G. T. Svacha, E. Mazur, S. Muller, C. Ronning, € D. Konjhodzic and F. Marlowet, Nano Lett., 7 (2007) 675.

[18] P. G. Collins, A. Zettl, H. Bando, A. Thess and R. E. Smalley, Science, 278 (1997) 100.

[19] J. Xiang, W. Lu, Y. Hu, Y. Wu, H. Yan and C. M. Lieber, Nature, 441 (2006) 489.

[20] C. Falconi, A. D'Amico and Z. L. Wang, Sensors and Actuators B, 127 (2007) 54.

[21] J. Gamby, J. P. Abid, B. Tribollet and H. H. Girault, Small, 4 (2008) 802.

[22] W. C. W. Chan and S. M. Nie, Science, 281 (1998) 2016.

[23] A. M. Smith, H. W. Duan, A. M. Mohs and S. M. Nie, Adv. Drug Delivery Rev., 60 (2008) 1226.

[24] Y. B. Mao, T. J. Park, F. Zhang, H. J. Zhou and S. S. Wong, Small, 3 (2007) 1122.

[25] J. P. Xie, J. Y. Lee, D. I. C. Wang and Y. P. Ting, ACS nano, 1 (2007) 429.

[26] P. Raveendran, J. Fu and S. L. Wallen, Green Chem., 8 (2006) 34.

[27] L. C. McKenzie and J. E. Hutchison, Chem. Today, 22 (2004) 30.

[28] Z. W. Pan, Z. R. Dai and Z. L. Wang, Science, 291 (2001) 1947.

[29] Y. Wu, J. Xiang, C. Yang, W. Lu and C. M. Lieber, Nature, 430 (2004) 61.

[30] J. E. Lee, S. M. Oh and D. W. Park, Thin Solid Films, 457 (2004) 230.

[31] Y. J. Tian, Y. P. Jia, Y. J. Bao and Y. F. Chen, Diam. Rel. Mater., 16 (2007) 302.

[32] D. Kuscer, J. Holc and M. Kosec, J. Am. Ceramic Soc., 90 (2007) 29.

[33] T. P. Yadav, N. K. Mukhopadhyay and R. S. Tiwari, J. Nanosci. Nanotech., 7 (2007) 575.

[34] M. Cernea, O. Monnereau, P. Llewellyn, L. Tortet and C. Galassi, J. Eur. Ceramic Soc., 26 (2006) 3241.

[35] A. Hartridge and A. K. Bhattacharya, J. Phys. Chem. Solids, 63 (2002) 441.

[36] X. Zhang and K. Y. Chan, Chem. Mater., 15 (2003) 451.

[37] A. S. Deshpande, N. Pinna, P. Beato, M. Antonietti and M. Niederberger, Chem. Mater., 16 (2004) 2599.

[38] B. B. Lakshmi, C. J. Patrissi and C. R. Martin, Chem. Mater., 9 (1997) 2544.

[39] H. Song, R. M. Rioux, J. D. Hoefelmeyer, R. Komor, K. Niesz, M. Grass, P. Yang and G. A. Somorjai, J. Am. Chem. Soc., 128 (2006) 3027.

[40] H. G. Yang, C. H. Sun, S. Z. Qiao, J. Zou, G. Liu, S. C. Smith, H. M. Cheng and G. Q. Lu, Nature, 453 (2008) 638.

[41] A. W. Xu, Y. P. Fang, L. P. You and H. Q. Liu, J. Am. Chem. Soc., 125 (2003) 1494.

[42] L. E. Greene, B. D. Yuhas, M. Law and P. Yang, Inorg. Chem., 45 (2006) 7535.

[43] K. B. Zhou, X. Wang, X. M. Sun, Q. Peng and Y. D. Li, J. Catalysis, 229 (2005) 206.

[44] X. Wang, J. Zhuang, Q. Peng and Y. D. Li, Nature, 437 (2005) 121.

Chapter 2

Experimental Details

2.1 Synthesis of Nanomaterials

Nanomaterials deal with very fine structures: a nanometer is a billionth of a meter. This indeed allows us to think in both the 'bottom up' or the 'top down' approaches to synthesize nanomaterials, i.e. either to assemble atoms together or to dis-assemble (break, or dissociate) bulk solids into finer pieces until they are constituted of only a few atoms. This domain is a pure example of interdisciplinary work encompassing physics, chemistry, and engineering up to medicine. There are two general approaches for the synthesis of nanomaterials and fabrication of nanostructure. Bottom –up can be further sub divided into four groups shown in Figure 2.1.

(a) Bottom-up approach
(b) Top-down approach

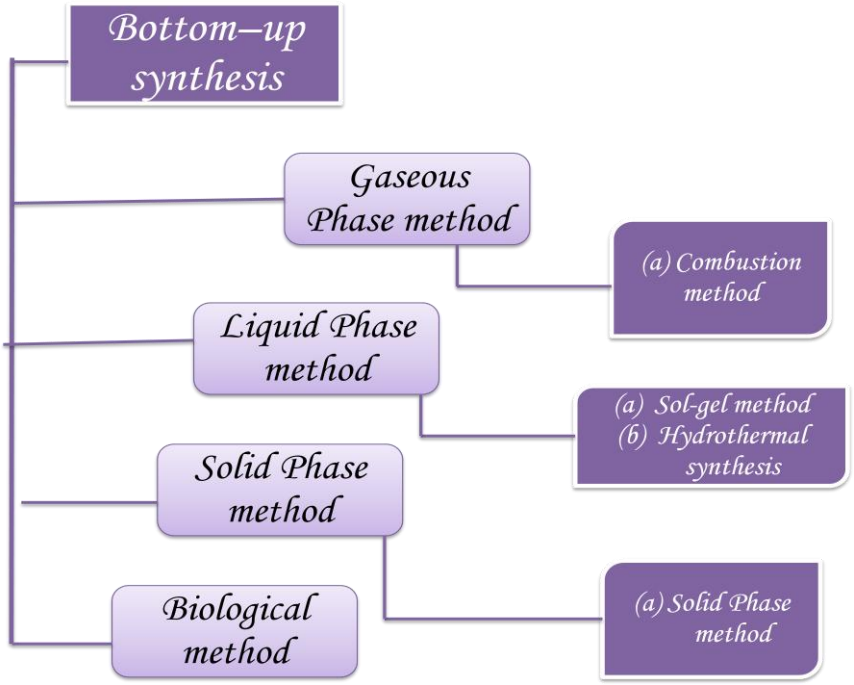

Figure 2.1 Classification of bottom-up approach

2.1.1 Hydrothermal synthesis

Hydrothermal synthesis is a process that utilizes single or heterogeneous phase reactions in aqueous media at elevated temperature (T>25ºC) and pressure (P>100 kPa) to crystallize materials directly from solution. Synthesis is usually conducted at autogenously pressure, which corresponds to the saturated vapor pressure of the solution at the specified temperature and composition of the hydrothermal solution. Upper limits of hydrothermal synthesis extend to over 1000ºC and 500 MPa pressures [82]. However, mild conditions are preferred for commercial processes where temperatures are less than 350ºC and pressures less than approximately 50 MPa. The transition from mild to severe conditions is determined mostly by corrosion and strength limits of the materials of construction that comprise the hydrothermal reaction vessels. The crystal growth is performed in a reaction pressure vessel called autoclave. Figure 2.2 shows the synthesis step involved in hydrothermal process.

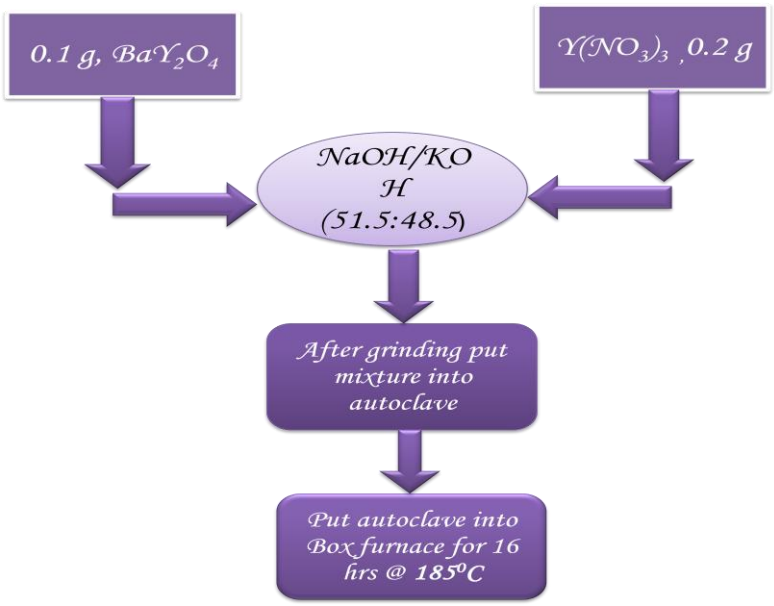

Figure 2.2:The synthesis step involved in hydrothermal process.

2.1.2 Sol-gel synthesis

Sol-gel processing refers to the hydrolysis and condensation of alkoxide-based precursors such as $Si(OEt)_4$ (tetraethylorthosilicate, or TEOS). The reactions involved in the sol-gel chemistry based on the hydrolysis and condensation of metal alkoxides M(OR)**z** can be described as follows:

Hydrolysis:

$$MOR + H2O \rightarrow MOH + ROH \text{ (hydrolysis)}$$

Condensation:

$$MOH + ROM \rightarrow M\text{-}O\text{-}M + ROH \text{ (condensation)}$$

Sol-gel method of synthesizing nanomaterials is very popular amongst chemists and is widely employed to prepare oxide materials. The sol-gel process can be characterized by a series of distinct steps

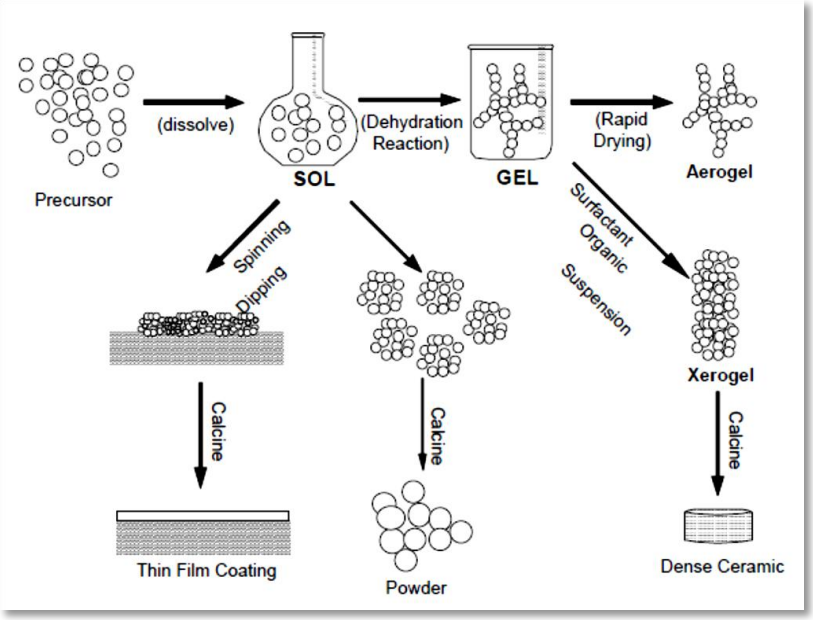

Figure 1.3 Schematic representation of sol-gel process of synthesis of nanomaterials

2.1.3 Combustion method

Combustion synthesis (CS) or self-propagating high-temperature synthesis (SHS) is an effective, low-cost method for production of various industrially useful materials. In the combustion synthesis exothermic reactions between metal nitrates and fuels such as urea are exploited [1].

The process involves the exothermic reaction of an oxidizer such as metal nitrates, ammonium nitrate, and ammonium perchlorate [2], and an organic fuel, typically urea (CH_4N_2O), carbohydrazide (CH_6N_4O), or glycine ($C_2H_5NO_2$).

The combustion reaction is initiated in a muffle furnace or on a hot plate at temperatures around 500 ^oC or less; much lower than the phase transition of the target material. In a typical reaction, the precursor mixture of water, metal nitrates, and fuel decomposes, dehydrates, and ruptures into a flame after about 3–5 min. The resultant product is a voluminous, foamy mass which occupies the entire volume of the reaction vessel. The chemical energy released from the exothermic reaction between the metal nitrates and fuel can rapidly heat the system to higher temperatures (~1600 ^oC) without an external heat source.

Nitrate to fuel ratio can be adjusted to vary the temperature generated. Highest temperatures are attained when this ratio is such that the oxidising and reducing valencies of the oxidisers and fuel are balanced. In general, a good fuel should react non-violently, produce non-toxic gases, and act as a complexing agent for metal cations [2]. Complexes increase the solubility of metal cations, thereby preventing preferential crystallization as the water in the precursor solution evaporates [3]. Combustion synthesis is also known as ***propellant synthesis, thermally explosive synthesis, auto-ignition,*** etc. Combustion synthesis processes are characterized by high-temperatures, fast heating rates and short reaction times.

It is well recognized fact that the fuel is an important component for combustion synthesis of nanoparticles. Urea and glycine are the most popular and attractive fuels for producing highly uniform, complex oxide ceramic powders with precisely controlled stoichiometry.

The difference in particle sizes with the use of different fuels depends upon the number of moles of gaseous products released during combustion. As more gases are liberated, the agglomerates are disintegrated and more heat is carried from the system thereby hindering particle growth.

Combustion synthesized powders are generally more homogeneous, have fewer impurities, and have higher surface areas than powders prepared by conventional solid-state methods [2]. The mechanism of the combustion reaction is quite complex. The parameters that influence the reaction include: type of fuel, fuel to oxidizer ratio, use of excess oxidizer, ignition temperature, and water content of the precursor mixture.

2.1.4 Solid State Reaction

Steps in Conventional Solid State Synthesis

1. Select appropriate starting materials.

a) Fine grain powders to maximize surface area.

b) Reactive starting reagents are better than inert.

c) Well defined compositions.

2). Weigh out starting materials

3). Mix starting materials together

a) Agate mortar and pestle (organic solvent optional)

b) Ball Mill (Especially for large preps > 20g)

4). Pelletize

5). Select sample container.

Reactivity, strength, cost, ductility are all important

a) Ceramic refractories (crucibles and boats)

$Al_2O_3$1950 °C

b) Precious Metals (crucibles, boats and tubes)

Pt 1770 °C

c) Sealed Tubes

SiO2- Quartz, Au, Ag, Pt

6) Heat

a) Factors influencing choice of temperature for volatilization

b) Initial heating cycle to lower temperature can help to prevent spillage and volatilization

c) Atmosphere is also critical

Oxides (Oxidizing Conditions) – Air, O_2, Low Temps

Oxides (Reducing Conditions) – H2/Ar, CO/CO2, High T

Nitrides – NH_3

or Inert (N_2, Ar, etc.)

Sulfides – H_2S

Sealed tube reactions, Vacuum furnaces

7) Grind product and analyze (x-ray powder diffraction)

8) If reaction incomplete, return to step 4 and repeat.

2.2 Characterization Techniques

2.2.1 X- Ray Diffraction

X-ray diffraction (XRD) is a powerful technique used to uniquely identify the crystalline phases present in materials and to measure the structural properties (strain state, grain size, epitaxial, phase composition, preferred orientation, and defect structure) of these phases. In X-ray diffraction (XRD) a collimated beam of X-rays, with wavelength λ~0.5-2Å, is incident on a specimen and is diffracted by the crystalline planes in the specimen according to Bragg's law ($\lambda = 2d \sin\theta$, where d is the spacing between atomic planes in the crystalline phase). The intensity of the diffracted X-rays is measured as a function of the diffraction angle 2θ and the specimen's orientation.

To determine the phase purity of the QDs synthesized in the current work, the crystalline data was obtained by X-ray diffractometer (XRD); Bruker-AXS D8 Advance system using Cu Kα (λ ~1.54056 Å) with step size of 0.01 at 0.15 steps/s. The characterizations were

performed at National Physical Laboratory (NPL). New Delhi. Figure 2.4 shows the photograph of the XRD Bruker-AXS D8 at NPL.

Figure 2.4: X-Ray Diffractometer (Bruker's AXS D8).

2.2.2 Scanning Electron Microscope (SEM)

The Scanning Electron Microscope (SEM) is often the first analytical instrument used when a "*quick look*" at a material is required. In the SEM an electron beam is focused into a fine probe and subsequently raster scanned over a small rectangular area. As the beam interacts with the sample it creates various signals (secondary electrons, internal currents, photon emission, etc.), all of which can be appropriately detected. These signals are highly localized to the area directly under the beam. By using these signals to modulate the brightness of a cathode ray tube, which is raster scanned in synchronism with the electron beam, an image is formed on the screen. This image is highly magnified and usually has the "*look*" of a traditional microscopic image but with a much greater depth of field. With ancillary detectors, the instrument is capable of elemental analysis. The resolution of the

SEM can approach a few nm and it can operate at magnifications that are easily adjusted from about 10-300,000X.

The SEM analysis of the samples in the current work, were carried out using Zeiss EVO MA-10 SEM at NPL, New Delhi. The resolution of SEM was 20 nm at 30kV with magnification varying between 5-1,000,000X. A photograph of the same has been presented in figure 2.5.

Figure 2.5: Scanning electron microscope (SEM).

2.2.3 Energy Dispersive X-ray Spectroscope (EDX)

Energy-dispersive X-ray spectroscopy is used for quality control and test analysis in many industries including: computers, semiconductors, metals, cement, paper, and polymers. EDX is also being used in medicine in the analysis of blood, tissues, bones, and organs; in pollution control, for asbestos identification; in field studies including ore prospecting, archaeology and oceanography; for identification and forgery detection in the fine arts; and for forensic analysis in law enforcement. With a radioactive source, EDX system is easily

portable and can be used in the field more easily than most other spectroscopy techniques. The main advantages of EDX are its speed of data collection; the detector's efficiency (both analytical and geometrical); the ease of use; its portability; and the relative ease of interfacing with existing equipment.

Besides several advantages, there are a few disadvantages of the EDX systems. For example, these have poor energy resolution of the peaks, (a typical EDX peak is about 100x the natural peak width, limited by the statistics of electron-hole pair production and electronic noise, which often leads to severe peak overlaps); a relatively low peak-to-background ratio in electron-beam instruments due to the high background coming from *Bremsstrahlung* radiation emitted by electrons suffering deceleration on scattering by atoms; and a limit on the input signal rate because of pulse processing requirements.

2.2.4 UV-VIS-NIR Spectrophotometer

Ultraviolet-visible-near infra red spectroscopy (UV-VIS-NIR) refers to absorption spectroscopy or reflectance spectroscopy in the ultraviolet-visible spectral region. This means it uses light in the visible and adjacent (near-UV and near-infrared (NIR)) ranges. The absorption or reflectance in the visible range directly affects the perceived color of the chemicals involved. In this region of the electromagnetic spectrum, molecules undergo electronic transitions. This technique is complementary to fluorescence spectroscopy, in that fluorescence deals with transitions from the excited state to the ground state, while absorption measures transitions from the ground state to the excited state.

A typical UV-VIS-NIR instrument consists of a source, wavelength disperser, sample holder, detector and readout such as computer. Absorption or the reflectance is measured by comparing the sample's response with a blank space. Figure 2.6 illustrates a block diagram for a typical UV-VIS instrument.

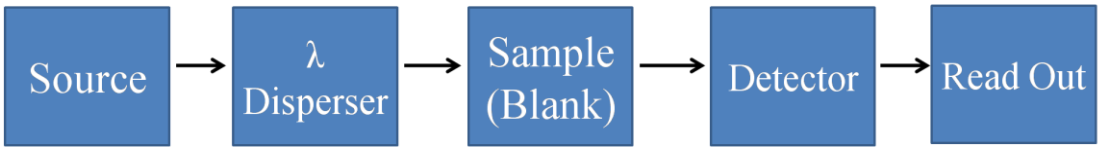

Figure 2.6: Block diagram for a typical UV-VIS instrument

In the current work a UV-VIS spectrophotometer, the Hitachi model no. U-3900H was used. The instrument has a WI lamp (visible region) and a D2 lamp (UV region) as light sources for selective use according to measuring wavelength range. Here, double beam optics is used for the stable measurements, in which the monochromatic beam selected with a monochromator, splits into reference beam and sample beam with a rotating mirror and the beams are directed into the sample compartment. Figure 2.7shows the photograph of the UV-VIS instrument used in the current study. This study was also carried out at NPL, Delhi.

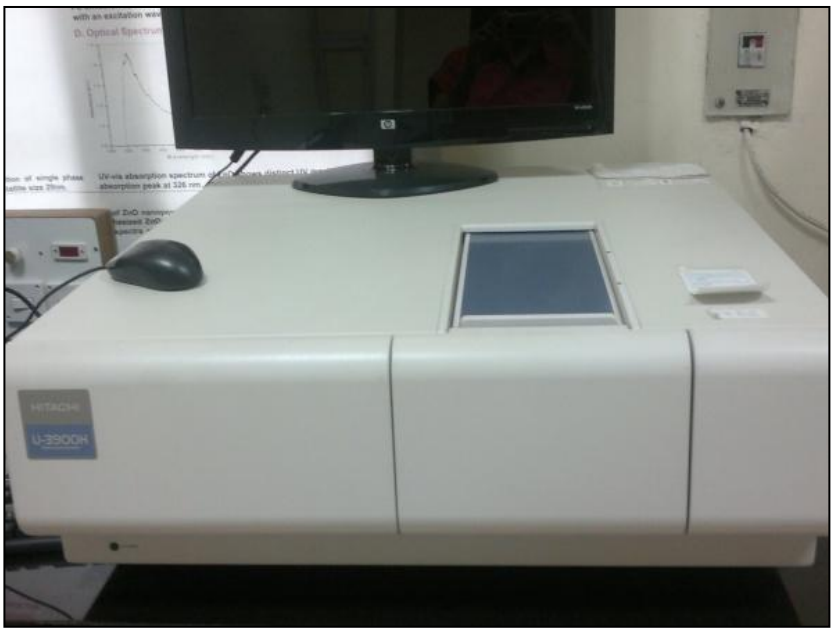

Figure 2.7: UV-VIS-NIR spectrophotometer

2.2.5 Thermal Gravimetric Analysis

Thermogravimetric analysis (TGA) is an analytical technique used to determine a material's thermal stability and its fraction of volatile components by monitoring the weight change that occurs as a specimen is heated. The measurement is normally carried out in air or in an inert atmosphere, such as Helium or Argon, and the weight is recorded as a function of increasing temperature. In addition to weight changes, some instruments also record the temperature difference between the specimen and one or more reference pans (differential thermal analysis, or DTA) or the heat flow into the specimen pan compared to that of the reference pan (differential scanning calorimetry, or DSC). The latter can be used to monitor the energy released or absorbed via chemical reactions during the heating process. The TGA/ SDTA851 make: Mettler TOLEDO at NPL was used for TGA measurements

2.2.6 Atomic Absorption Spectroscope (AAS)

Atomic absorption spectroscopy (AAS) is a common technique used in many analytical chemistry protocols, as well as in applications requiring a high degree of precision and accuracy, such as food and drug safety, clinical diagnostics, and environmental sampling. Atomic absorption spectrometers may be used to analyze the concentration of over 70 different elements in a given sample solution, making these a very valuable instrument in any laboratory procedure that requires reliable measurements and reproducibility.

When using atomic absorption spectroscopy as an analytical technique the absorption of light of free atoms is measured. Therefore, it is one of the branches of atomic spectroscopy, together with flame photometry. Flame photometry measures the intensity of light emitted by free atoms when their electrons return to ground state after the excitation by light. However unlike flame photometry AAS is based on the "first half" of the excitation process, while atoms absorb light getting their electrons from the ground state to a higher energy level. Although the atomic absorption spectrophotometer is quite expensive, the technique is very wide-spread. The sample is atomised at a very high temperature (2500 ^{o}C

-3000 ºC) and the free atoms have line spectrum. It means that they can only absorb the energy of light at discrete energy levels according to the excitations of electrons. Excitation energies in this case are determined by the difference between the energy level of the ground state and one of the excitation states of their electrons. Only a light with a concrete wavelength belongs to each of these excitation energies and when this light is absorbed it is missing from the continuous spectra of the electromagnetic radiation: a black line appears in the absorption spectrum of the atom. There are no vibration or rotation energy levels that would widen the lines to bands in the spectrum. Using AAS, free atoms are *lit* by monochromatic light (called *resonance radiation* that has got a special wavelength) that belongs to one line of their spectrum and therefore it has the suitable excitation energy mentioned above. Only the examined atoms can absorb it. As a result of absorption, the intensity of light decreases, as it is proportional to the number of the examined atoms being present. That makes very sensitive quantitative measurements possible.

The AAS spectroscopy for the samples prepared in the current work has been carried out using the Varian 6 system shown in figure 2.8 from Analytikjena at NPL, New Delhi.

Figure 2.8: Atomic absorption spectrometer.

2.2.7 Photoluminescence Spectrometer (PL)

In photoluminescence (PL) measurements electronic properties of a material is probed non-destructively, by using photons to excite its electronic states and then analyzing the optical emission as the system relaxes. Typically, higher energy photons are directed onto the sample for excitation, and the emitted luminescence is collected by a lens and focused to a photo-detector.

The spectral energy distribution and time dependence of the emission are related to electronic transition probabilities within the sample, and can be used to provide qualitative and, sometimes, quantitative information about chemical composition, structure (bonding, disorder, interfaces, quantum wells), impurities, kinetic processes, and energy transfer.

Figure 2.9 shows PL spectrometer from Edinburgh Instruments, UK (model F900) at NPL, New Delhi. The same instrument was used to measure the PL and time decay spectra of all the samples in the present work.

The spectrometer uses a Xenon lamp with monochromator to excite the samples for PL study. Microsecond xenon flash lamp and a nanosecond hydrogen flash lamp is used as source of excitations for time decay measurements of samples.A typical configuration of the spectrometer is schematically described in figure 2.10

The excitation monochromator isolates a band of a particular wavelength from the light from the xenon lamp to obtain excitation light. Since brighter excitation light will contribute to higher sensitivity of the spectrometer, the excitation monochromator incorporates a diffraction grating with a larger aperture to collect the largest possible amount of light. The sample holder holds a cell filled with sample. The emission monochromator selectively receives fluorescence emitted from the sample and its photomultiplier tube measures the intensity of the fluorescence. This monochromator has a diffraction grating whose size is the same as that of the excitation monochromator to collect the greatest possible amount of light.

Figure 2.9: Photoluminescence Spectrometer

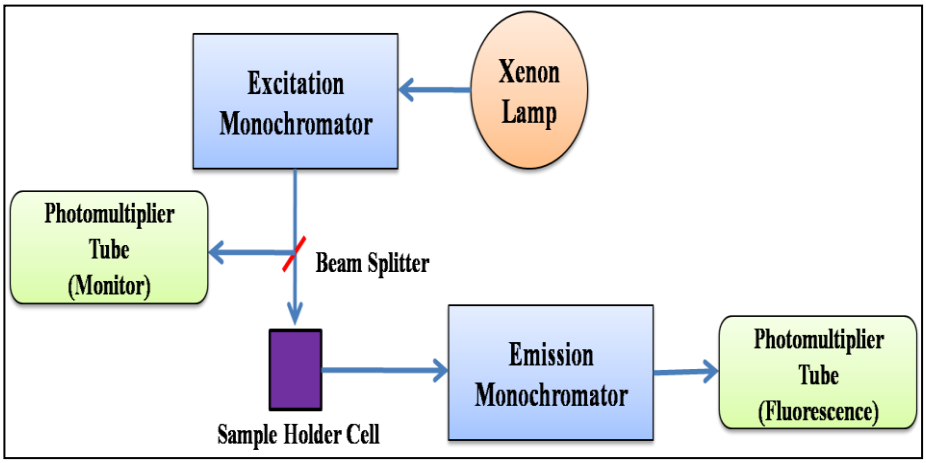

Figure 2.10: Constitution of a photoluminescence spectrophotometer.

The photomultiplier tube is for monitoring. Generally, the xenon lamps used on spectrophotometer are characterized by very high emission intensity and an uninterrupted radiation spectrum. The non-uniformity in the radiation spectrum of the xenon lamp and in the spectral sensitivity characteristics of the photomultiplier tube (called instrument functions) causes distortion in the spectrum. To overcome these factors, the photomultiplier tube monitors a portion of excitation light and feeds the resultant signal back to the photomultiplier tube for fluorescence scanning. (This scheme is called the light-source compensation system.) This concludes the description about the synthesis methods and characterization tools used in the current work. The methods adapted to make device and its testing has been presented in the subsequent sections.

References

[1] K.C. Patil et al. / Current Opinion in Solid State and Materials Science 6 (2002) 507–512

[2] J.J. Kingsley, L.R. Pederson, Energetic materials in ceramics synthesis, Mat. Res. Soc. Symp. Proc. 296 (1993) 361–366.

[3] L.R. Pederson, G.D. Maupin, W.J. Weber, D.J. McCready, R.W. Stephens, Combustion synthesis of YBa2Cu3O7 x: glycine/metal nitrate method, Mater. Lett. 10 (9) (1991) 437–443

Chapter 3

Synthesis of ZnO Nanocrystals for Invisible Security Code Applications

3.1 Introduction

Zinc oxide (ZnO) and its various nanostructures have become materials of great interest these days [1-5]. Reasons being many, its wide direct band gap (3.37 eV or 375 nm at room temperature) and large exciton binding energy (60 meV) results in bright photoluminescence emission in the near ultraviolet region [6]. It shows various properties such as piezoelectricity, pyroelectricity, luminescence, semiconducting and catalytic activity due to which it is being used in wide range of applications including spintronics, varistors, laser diodes, LEDs, cosmetics, gas sensors, photocatalysis, an additive in paints as well as in memory and optoelectronic devices [7-11]. Its various nanostructure morphologies find immense applications in different fields. Many methods have been investigated so far for the synthesis of size-controlled ZnO nanocrystals via co-precipitation, sol-gel, hydrothermal, electrodeposition, chemical vapour deposition, micro-emulsion etc. [12-18]. In all those synthesis methods, yield of the nanocrystal is a serious issue. In order to exploit size-controlled ZnO nanocrystals for any large-scale application, the yield of the nanocrystal should be sufficiently enough. We herewith report a novel citrate-gel incineration method to produce size-controlled ZnO nanocrystals in narrow size distribution. Moreover, it provides several advantages over other methods such as high purity of products, high yield, short reaction time, relative simplicity of the process and inexpensive precursor chemicals. Incineration synthesis is a self-propagating high-temperature synthesis and it is an effective, low-cost method as it utilizes the exothermicity of redox chemical reaction for production of various industrially important nanocrystals [19,20]. This process involves a self-sustained reaction in homogeneous solution of different oxidizers (e.g. metal nitrates) and fuels (e.g. urea, glycine, hydrazide and citric acid) [21]. Auto-incineration processing has been applied to the synthesis of variety of nanocrystals including Al_2O_3, ZrO_2, $MgAl_2O_4$, $BaTiO_3$ and many other phosphor materials such as $Y_3Al_5O_{12}:Eu^{3+}$, $ZnO:Cu^{2+}$, $SrAl_2O_4:Eu^{2+}$, Sr_2CeO etc. [22-24]. The literature concerning for the synthesis of these compounds mostly deals with the use metal nitrates as precursors [25]. Unfortunately the researchers paid least attention on the selection of

precursor chemicals used for the synthesis of nanocrystals, rather concentrated more on thermal and non-thermal processing parameters governing the reaction. That's why in this present work we tried to explore the effect of various precursor chemicals on crystallite size, morphology and luminescence properties of ZnO nanocrystals and relevant theory has been discussed. Moreover as purity of ZnO is important for its application, generally heat treatment is done **for** the samples prepared by various wet chemical routes, to eliminate organic species adsorbed on the surface of ZnO but nanocrystals synthesized by incineration do not really require further heat treatment and are highly pure.

3.2 Experimental Section

(a) Preparation:

ZnO nanocrystals were synthesized by the sol-gel incineration method as discussed in section 2.1.2.

(b) Characterization:

Thermal analysis was carried by simultaneous thermogravimetric analysis (TGA) and differential scanning calorimetry (DSC) under constant Ar gas flow with a heating rate of 10°C min^{-1}. The phase purity was checked by x-ray powder diffractometer of Bruker D-8 make with Cu Kα radiation operated at 35 kV and 30 mA. Microstructures of the nanocrystal samples were observed using scanning electron microscope (SEM, Zeiss EVA MO-10). The photoluminescence (PL) spectra were recorded using an Edinburgh Luminescence Spectrometer (Model: F900) fitted with a xenon lamp in the scan range from 200-800 nm at room temperature.

3.3 Results and Discussion

(a) Thermal analysis:

Figure 3.1 shows the TGA/DSC curves confirming the breaking down of organic molecules i.e. decomposition of citric acid in the gel complex. Sample studied was made by zinc acetate precursor. Gel of citric acid and zinc acetate was thermally treated at 900°C at heating rate of 10°C/min. The first endothermic event occurred between 150 and 200°C which can be associated with the removal of surface water. At a temperature of ~190°C the weight loss was maximum.

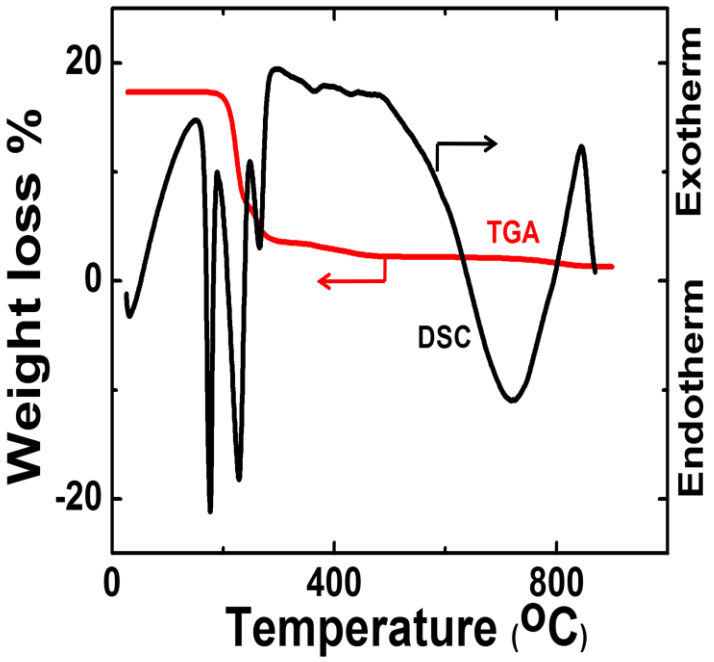

Figure 3.1: TGA/DSC curve for thermal decomposition of mixture of zinc acetate and citric acid

TGA curve shows the weight loss in two steps at 200 and 280°C. The weight loss of 58% occurred at 200°C and a loss of 22% at 280°C.

The endotherms observed at these temperatures may be due to removal of organic species present over the surface of ZnO nanocrystals [26]. A sharp endothermic peak at 275°C was due to decomposition of anhydrous zinc acetate. There is a gradual loss observed at temperatures between 170 and 300°C which could be due to continuous release of organic molecules. A derivative weight loss curve can be used to convey the point at which weight loss is most apparent. The overall weight loss during the thermal decomposition is 92.4% up to 900^{o}C. Beyond this temperature, no further weight loss has been observed. A similar trend has been observed when the precursor chemicals such as chloride, nitrate and sulphate were studied for TGA/DSC analysis. Hence, 900°C was fixed as furnace temperature for further studies.

(b) Powder X-ray diffraction (XRD) analysis:

Figure 3.2 shows the XRD pattern of ZnO nanocrystals prepared with different precursor chemicals. The diffraction pattern consists of peaks primarily associated with ZnO and no other spurious peaks were observed. The characteristic peaks attributed to hexagonal wurtzite ZnO nanocrystals were identified and marked in figure 3.2 (a).

All the diffraction peaks were found to be well matched with standard JCPDS data card file no. 36-1451. The broadness of the diffraction peaks indicates that the material is in nano-regime.

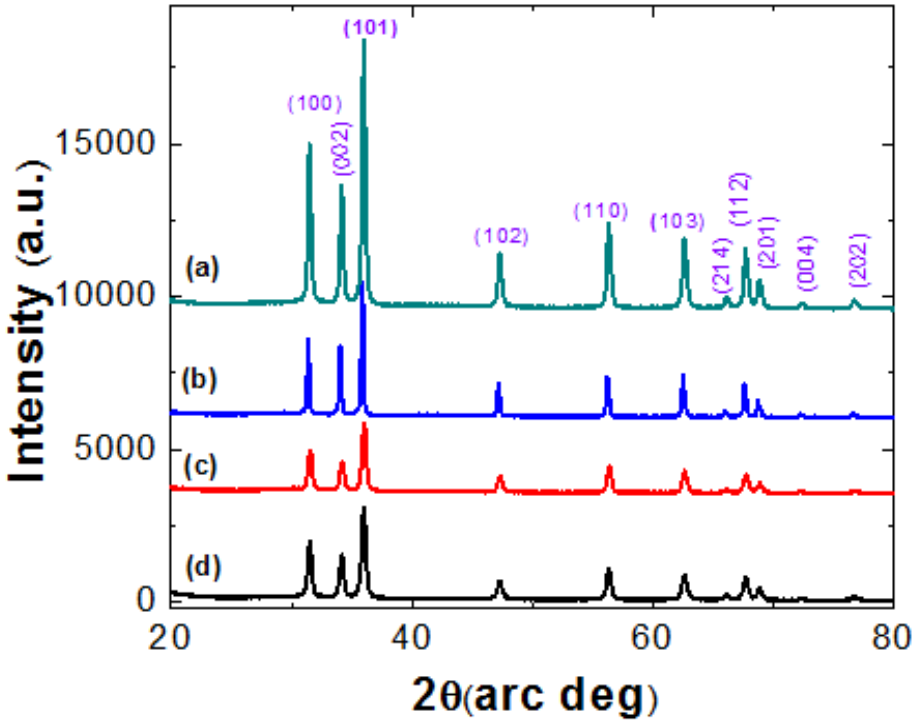

Figure 3.2: (a-d). (Color online) X-ray diffraction pattern of ZnO nanocrystals prepared using different precursor chemicals (a) Zinc acetate, (b) Zinc chloride, (c) Zinc sulphate monohydrate, (d) Zinc nitrate hexahydrate.

The existence of characteristic diffraction peaks at expected Bragg angles indicate that the nanocrystalline nature of the particles and the average crystallite size of these samples calculated were shown in Table 3.1. One can see the variation of crystallite size in accordance with the precursor chemical used. Minimum crystallite size has been obtained for zinc acetate and maximum for zinc chloride as precursor chemicals. Mean crystallite size (D_p) has been calculated using Debye-Scherrer equation [27]:

$$D_p = \frac{0.94\lambda}{\beta_{1/2}\cos\theta}$$

where $\beta_{1/2}$ is the full width at half maximum (FWHM) of the peaks in radian, θ is the Bragg angle and λ is the x-ray wavelength of Cu-Kα radiation.

Table 3.1: Calculated crystallite sizes of ZnO nanocrystals prepared from different precursor chemicals and their yield after sol-gel incineration technique.

Sample Code	Precursor salt	Avg. crystallite size (nm)	Yield of ZnO nanocrystals (%)
(a)	Zinc acetate	13.45	94
(b)	Zinc chloride	34.90	69
(c)	Zinc sulphate monohydrate	17.48	67
(d)	Zinc Nitrate hexahydrate	15.88	76

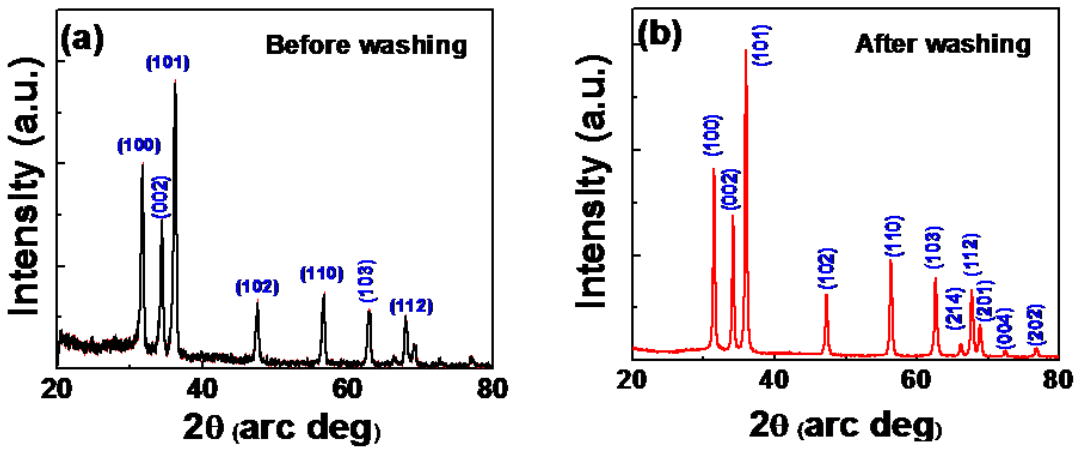

Figure 3.3: X-ray diffraction pattern of ZnO nanocrystals made from acetate precursor (a) before and (b) after repeated washings with ethyl alcohol.

Figure 3.3 represents the x-ray diffraction patterns of as synthesized ZnO nanocrystals and sample after repeated washing with ethyl alcohol. A few low intensity and spurious peaks were eliminated and slight broadening of major diffraction peaks were observed upon washing.

(c) Photoluminescence (PL) studies:

Room temperature photoluminescence (PL) spectra were recorded for the samples prepared using different zinc precursors. ZnO has two prominent transition peaks, one due to its band gap in near UV (375 nm or 3.37 eV at room temperature) region and other is broad band visible peak in the blue-green regions (between 450-520 nm). The PL excitation (PLE) peak corresponding to the UV region is attributed to the radiative recombination of excitons. Whereas the visible broad band appeared in the blue-green region is due to the intrinsic defects such as Zn_i, V_o, $O_{Zn,}$ V_{Zn} etc. [27]. In general, the relaxation of the photoexcitation of ZnO occurs via three processes: (i) recombination of electrons present in the conduction band and the hole present in the valance band, (ii) recombination of the electron-hole pair through defect levels resulting emission in the visible region and (iii) recombination of electron-hole pair through the surface states resulting into the non-radiative recombinations. In other words, the hole present in the valance band can be trapped to the surface states either by tunnelling to the defect levels within the band gap or may remain to the surface states. If the hole tunnels to the defect level and recombines to the electron it undergoes radiative recombination. Whereas if the hole doesn't tunnels it undergoes the non-radiative recombination with the surface trapped electron. Hence, the recombination process is dependent on the tunnelling probability of the surface trapped hole which in turn represents the characteristic of the host lattice. PL spectra of ZnO nanocrystals exhibit a deep level visible luminescence in addition to near band edge UV emission. Several mechanisms has been proposed for broad visible emission for ZnO such as due to the presence of singly ionized oxygen vacancies, multiple defect complexes, copper impurities, surface states and donor–acceptor complexes [6]. Green luminescence

(~2.28 eV) can be attributed to the transition between singly charged oxygen vacancy and photo excited hole or Zn interstitial related defects. The average particle size estimated from PL data for (a), (d) is ~12.8 nm whereas for sample (b) and (c) were 22 and 30 nm which is also evident from powder XRD studies. Bohr exciton radius for ZnO has been reported to be around 2 nm [28] which is less than the size of the particle and hence, the charge carriers experience a moderate quantum confinement effects however their recombination process was found out to be different from that of the bulk ZnO due to its high surface to volume ratio. Further emission of all samples lie in green region of visible spectra but with decrease in the size the PL emission occurs towards the blue region (~2.82 eV) of the spectra (i.e. when acetate and nitrate precursors were used). The quantum confinement of free exciton in nanostructures is expected to result in the blue shift of the emission peaks and size distribution would have lead to inhomogeneous broadening of exciton peak [29]. Blue shift observed for the samples (a) and (d) is maximum, whereas for sample (c) it is least. Intensity of emission spectra increases with decrease in the particle size and nanocrystals exhibit broad and Strokes-shifted bands, arising from the deep traps of the surface states as shown in Figure 3.4. Band gap of ZnO nanocrystals estimated from photoluminescence excitation spectra for the samples (a) and (d) were ~3.8 eV which is more than band gap of bulk ZnO (3.37 eV).

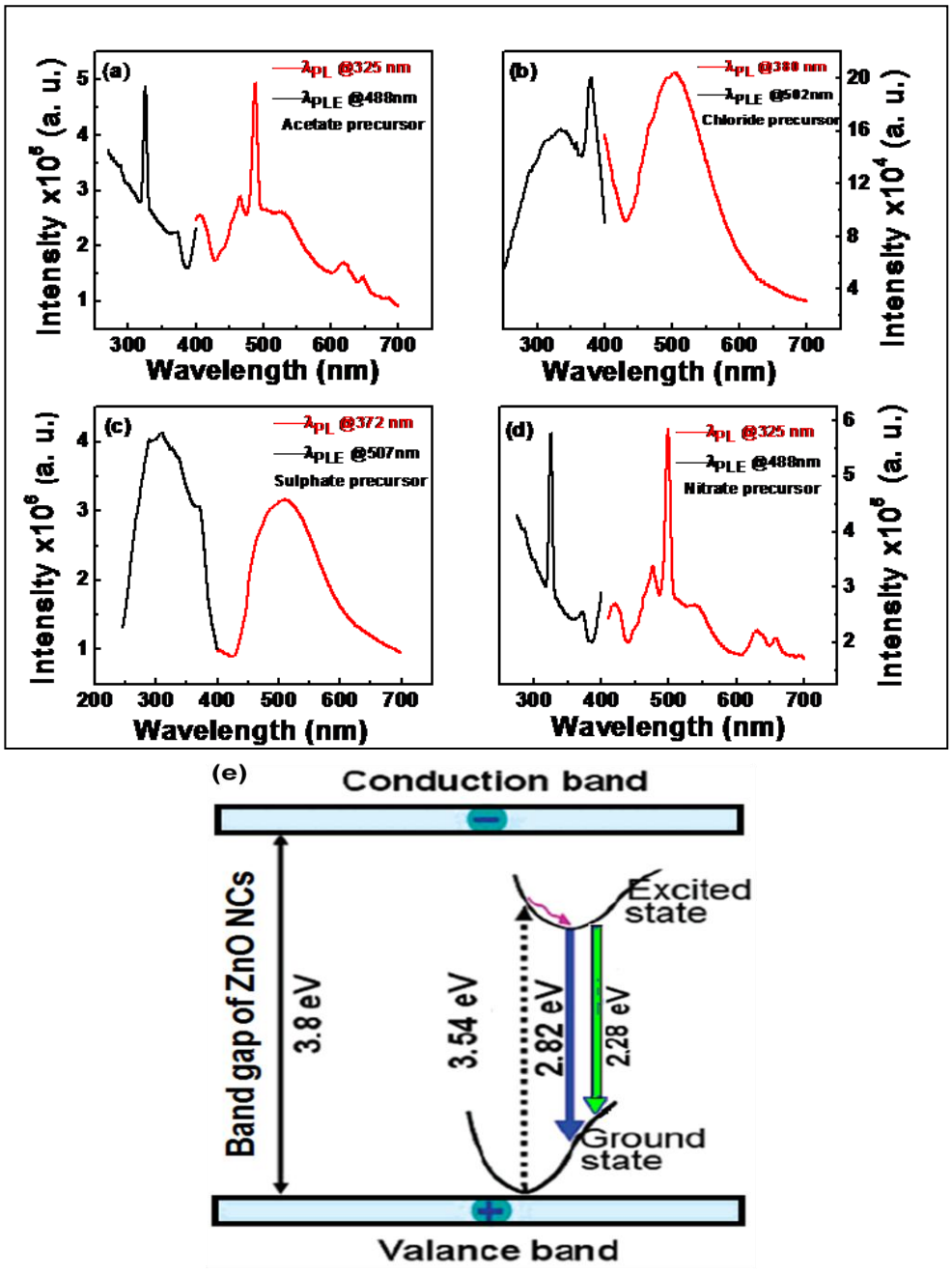

Figure 3.4: PL and PLE spectra of ZnO nanocrystals prepared using different precursor chemicals (a) zinc acetate, (b) zinc chloride, (c) zinc sulphate monohydrate, (d) zinc nitrate hexahydrate and (e) band energy diagram depicting the blue and green PL emissions.

(d) Scanning Electron Microscopy (SEM) observations:

In order to understand the surface morphology of ZnO nanocrystals, electron microscopy observations have been performed. Figure 3.5 shows the SEM images for all the samples made using different precursor chemicals. It was found out that ZnO nanocrystals were in the form of agglomerates with the nanocrystal size between 12 and 35 nm. It is interesting to observe that by mere variation of precursor chemicals, the nanocrystals of different morphologies and sizes were obtained. Sample (a) and (c) shows spherical nanocrystals whereas (b) shows cuboidal particles whereas (d) shows needle-like nanostructures. This is one of the few reports that depict the formation of needle-like nanostructures without the use of seeding particle. The size of the nanocrystals observed in the SEM images seems to be more than that observed from the powder XRD and photoluminescence measurements and the reason could be the tendency of agglomeration of very small size nanocrystals their high reactivity.

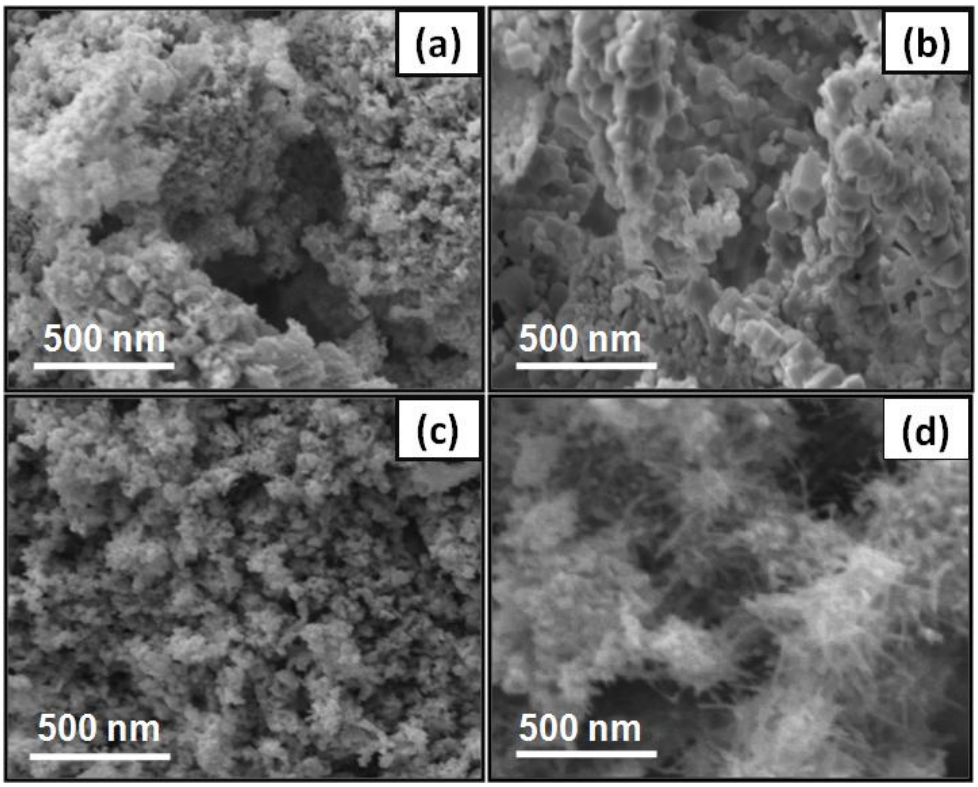

Figure 3.5: SEM images of ZnO nanocrystals prepared using different precursor chemicals (a) Zinc acetate, (b) Zinc chloride, (c) Zinc sulphate monohydrate, (d) Zinc nitrate hexahydrate.

(e) Aqueous Stability of ZnO Nanocrystals:

In the past few years, much attention has been devoted to the development of transparent and aqueous stable ZnO nanocrystals for various applications by carefully tailoring of their sizes and surface states. But scanty work has been reported on the high yield production of ZnO nanocrystals that are stable in water for at least six months. To the best of our knowledge, no serious attempt has been made to disperse ZnO nanocrystals without polymer encapsulation and obtain aqua stability.

In the present case, we have successfully demonstrated the preparation of a transparent and aqueous-stable ZnO nanocrystal colloid that can be used as a luminescent marker. For this 5% solution of trisodium citrate in water was taken at room temperature (~25 ^{o}C) to which ~10 mgcm^{-3} ZnO nanocrystal powder was added. The loading amount of the nanocrystals could be easily scaled up to 25 mg cm^{-3} by sacrificing the optical transparency. This property of ZnO nanocrystals suggests the easy fabrication of ZnO based EL devices by using techniques like spin casting and dip coating.

4.4 Conclusions:

Aqueous stable zero-dimensional pure ZnO nanocrystals have been synthesized by sol-gel incineration process. In the present study, effect of precursor chemicals on crystallite size, morphology and luminescent properties have been studied. ZnO nanocrystals prepared using zinc acetate as a precursor were found to have minimum crystallite size, spherical shaped nanocrystals and better luminescent properties as compared to other samples prepared using different precursor chemicals. Due to high surface to volume ratio of the

ZnO nanocrystals they have a higher concentration of surface defects which increases with decrease in the particle size. These defects may include loosely bound acetate/ nitrate/ chloride/sulphate anions on surface of the ZnO nanocrystals which might be the governing reason for the variation in the crystallite sizes, shapes and luminescent properties of as prepared ZnO nanocrystals.

References:

1. E. A. Meulekamp, *J. Phys. Chem. B*, 102 (1998) 5566.
2. Z. Y. Fan, J. G. Lu, *J. Nanosci. Nanotech,* 5 (2005) 1561.
3. G. C. Yi, C. R. Wang, W. I. Park, *Semicond. Sci. Technol.,* 20 (2005) S22.
4. B. Lo, J. Y. Chang, A. V. Ghule, S. H. Tzing, Y. C. Ling, *Scr. Mater.,* 54 (2006) 411.
5. R. Brayner, R. Ferrari-Iliou, N. Brivois, S. Djediat, M. F. Benedetti, F. Fievet, *Nano Lett.,* 6 (2006) 866.
6. A. B. Djurisic, W. C. H. Choy, V. A. L. Roy, Y. H. Leung, C. Y. Kwong, K. W. Cheah, T. K. G. Rao, W. K. Chan, H. F. Lui, C. Surya, *Adv. Funct. Mater*. 14 (2004) 856.
7. X. P. Shen, A. H. Yuan, Y. M. Hu, Y. Jiang, Z. Xu, Z. Hu, *Nanotechnology*, 16 (2005) 2039.
8. E. Monroy, F. Omnes, F. Calle, *Semiconduc. Sci. Technol.*, 18 (2003) R33.
9. Y. R. Ryu, T. S. Lee, J. A. Lubguman, H. W. White, Y. S. Park, C. J. Youn, *Appl. Phys. Lett.* 87 (2005) 153504.
10. X. Han, G. Wang, Q. Wang, L. Cao, R. Liu, B. Zou, J. G. Hou, *Appl. Phys. Lett.* 86 (2005) 223106.
11. A. Ohtomo, M. Kawasaki, H. Koimura, T. Yasuda, *Appl. Phys. Lett.*, 75 (1999) 980.
12. W. F. Shen, Y. Zhao, C. B. Zhang, *Thin Solid Films*, 483 (2005) 382.

13. S. H. Bae, S. Y. Lee, B. J. Jin, S. Im, *Appl. Surf. Sci.* 169 (2001) 525.

14. T. P. Niesen, M. R. De Guire, *J. Electroceram.*, 6 (2001) 169.

15. S. Chaudhuri, D. Bhattacharya, A. B. Maity, A. K. Pal, *Surf. Coat. Adv. Mater*. 246 (1997) 181.

16. D. Bahnemann, *Sol. Energy*, 77 (2004) 445.

17. Y. Lee, H. Kim, Y. Roh, *J. Appl. Phys.*, 40 (2001) 2423.

18. M. Berber, V. Bulto, R. Kliss, H. Hahn, *Ser. Mater.* 53 (2005) 547.

19. K. R. Venkatachari, D. Huang, S. P. Ostrander, W. A. Schulze, G. C. Stangle, *J. Mater. Res.*, 10(3) (1995) 748.

20. Z. A. Munir, U. Anselmi- Tamburini, *Mater Sci Reports* 3(7/8) (1989) 277.

21. P. K. Sharma, R. K. Dutta, M. Kumar, P. K. Singh, A. C. Pandey, V. N Singh, *IEEE Transactions on Nanotechnology* 10 (2011) 1.

22. J. Gomes, O. A. Serra, A. M. Pires, *Ecl. Quim*, 27 (2002) 187.

23. L. Sun, J. Yao, C. Liu, C. Liao, C. Yan, *J. Lumin.* 87-89 (2000) 447.

24. G. Tessari, M. Bettinelli, A. Speghini, D. Ajo, G. Pozza, L. E. Depero, B. Allieri, L. Sangaletti, *Appl. Surf. Sci.* 144-145 (1999) 686.

25. H. Chander, D. Haranath, V. Shanker, P. Sharma, *J. Cryst. Growth* 271 (2004) 307.

26. S. Fujihara, C. Sasaki, T. Kimura, *App. Surf. Sci.* 180 (2001) 341.

27. B. K. Sharma, N. Khare, D. Haranath, *Solid State Communication* 150 (2010) 2341.

28. Y Gu., I. L. Kuskovsky, M. Yin, S O'Brien and G. F. Neumark, *Appl. Phys. Lett.* 85 (2004) 17.

29. V. A. Fonoberov, K. A. Alim and A. A. Balandin, *Phys. Rev. 73 (*2006) 165317.

Chapter 4

Synthesis of Multicomponent Oxide Nanophosphors for LED Applications

4.1 Introduction

Hydrothermal powder synthesis has been known as a powerful method for the preparation of fine, high-purity, and homogeneous powders of various single-component and multicomponent oxide powders [1]. Furthermore, powders with particle sizes in the nanometer to centimeter range can be synthesized depending on the configuration of the hydrothermal equipment. Recently, multicomponent oxide powders, especially, perovskite type oxide powders, have attracted attention for their useful electronic applications such as dielectric, piezoelectric, electrostrictive, and transparent electro optic ceramics [2,3]. It has been commonly accepted that an unagglomerated spherical powder with a narrow size distribution is the most desirable state for the compacting and sintering of ceramics [4]. Generally, hydrothermal synthesis utilizes the treatment of aqueous solutions or suspensions of precursor gel powders at elevated temperatures and pressures.

4.2 Experimental Section

(a) Material synthesis

Complex oxide phosphors namely BaY_2O_4 and SrY_2O_4 were synthesized by the hydrothermal process as explained in section 2.1.1.

4.3 Results and Discussion

(a) Powder XRD Analysis

X-ray diffraction (XRD) spectra were recorded with high resolution using Cu Kα radiation (1.541841 Å). XRD spectra of the BaY_2O_4 and SrY_2O_4 are shown in the Figure 4.1 and 4.2 respectively. The prepared sample was found to match well with the reported data (JCPDS 82-2319) and (JCPDS 32-1272) with some peak shift due to effect of lattice strain.

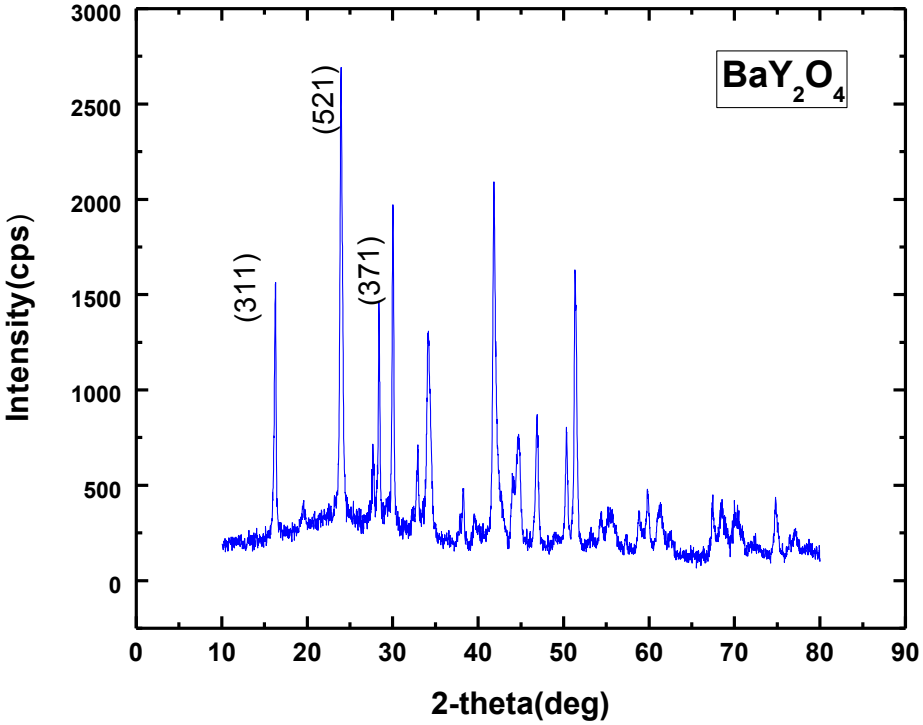

Figure 4.1 XRD of BaY_2O_4

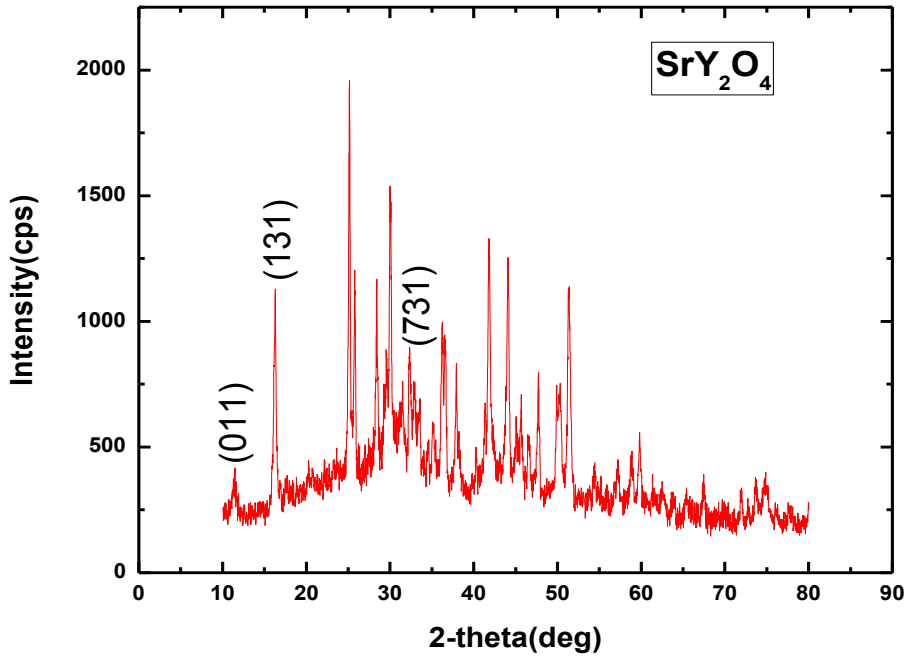

Figure 4.2: XRD of SrY_2O_4

(b) SEM observations

The surface morphological features of the powder nanophosphor were studied by scanning electron microscope (SEM). These images exhibited homogeneous aggregates of varying shapes and sizes.

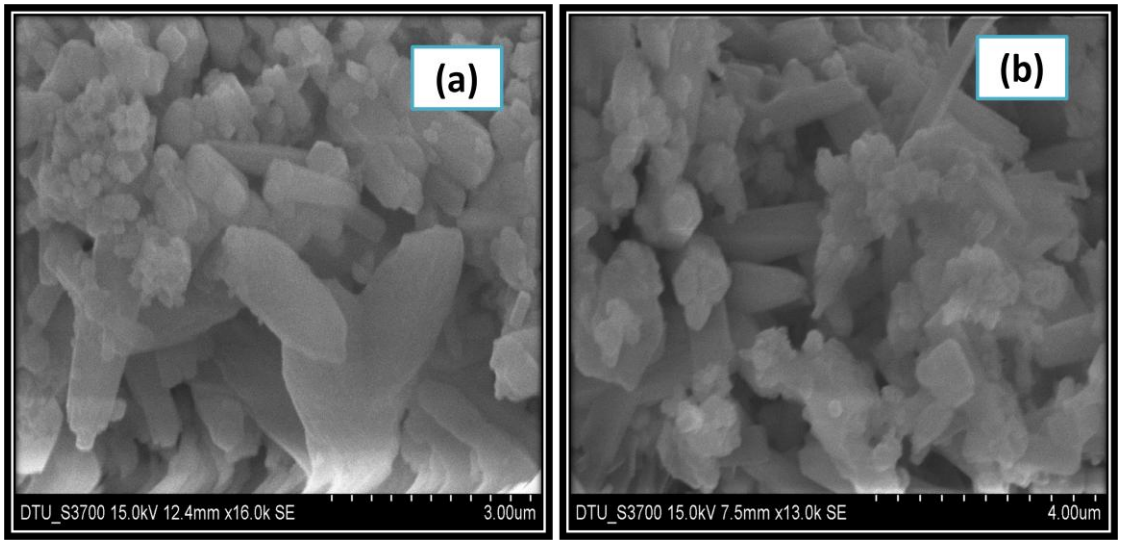

Figure4.3: SEM images of BaY_2O_4 at 16 and 13 kX magnifications

From figure 4.3 it has been found that BaY_2O_4 has rod type structure at 16 and 13 kX magnifications. It is interesting to observe that SrY_2O_4 in the figure 4.4 have nano-flower type structure at 2.7, 3.5 and 3.2 kX magnifications.

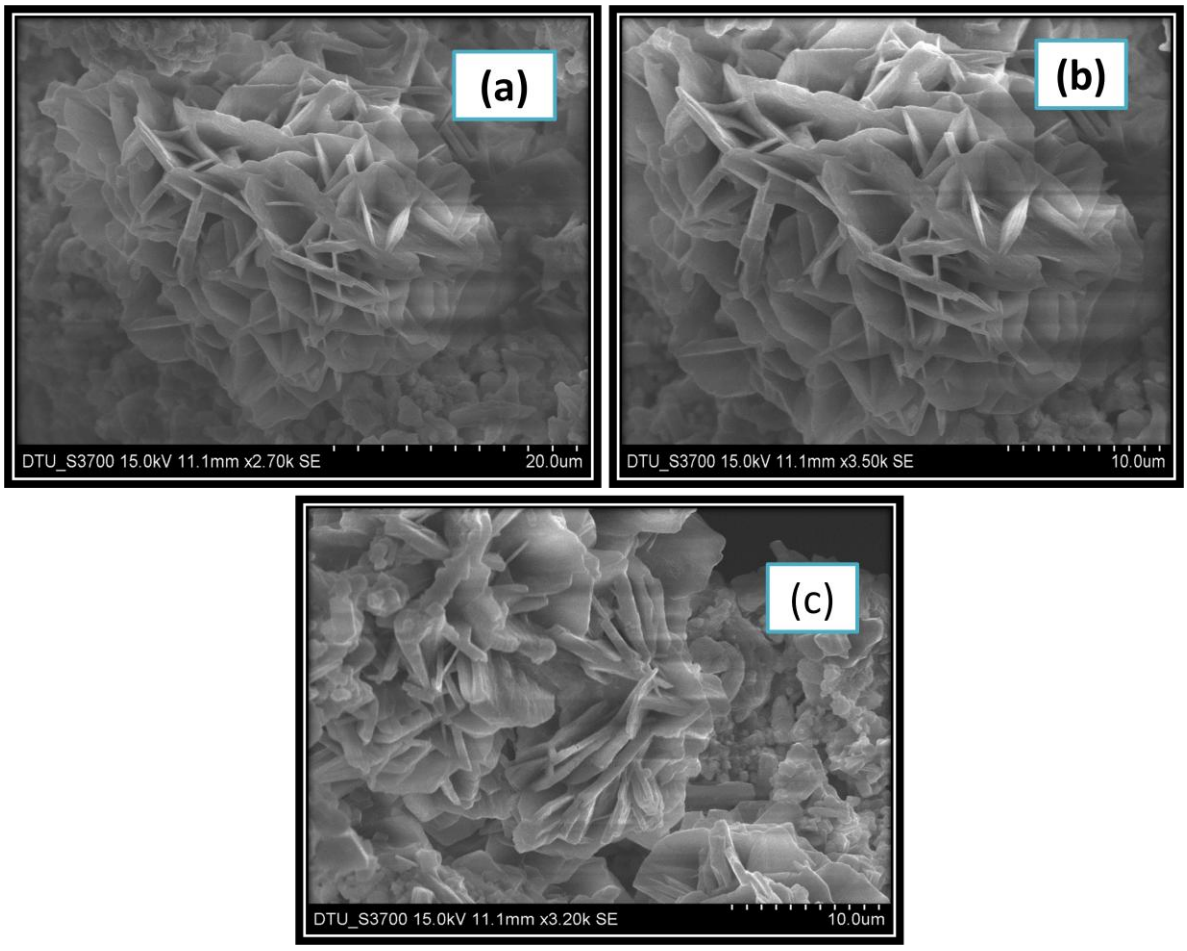

Figure 4.4: SEM Images of SrY_2O_4 at 2.7, 3.5 and 3.2 kX magnifications respectively

4.4 Conclusions

Multicomponent oxide phosphors are prepared by the hydrothermal synthesis using complex mediated approach. The method is based on a reaction between a metallic salt and a metallic oxide in a solution of molten mixed potassium hydroxide and sodium hydroxide eutectic at ~185 °C and normal atmosphere without using an organic dispersant or capping agent. This methodology provides a one-step, convenient, low-cost, nontoxic, and mass-production route for the synthesis of nanostructures of functional oxide materials of various structure.

References

[1] W. J. Dawson, ‘‘Hydrothermal Synthesis of Advanced Ceramic Powders,’’ *Am. Ceram. Soc. Bull.,* **67** [10] 1673 (1988) 78

[2] L. E. Cross, ‘‘Dielectric, Piezoelectric, and Ferroelectric Components,’’ *Am. Ceram. Soc. Bull.*, **63** [4] 586 (1984) 90

[3] K. S. Mazdiyasni, ‘‘Fine Particle Perovskite Processing,’’ *Am. Ceram. Soc. Bull.,* **63** 591(1984) 94

[4] W. H. Rhodes, ‘‘Agglomerate and Particle Size Effects on Sintering Yttria- Stabilized Zirconia,’’ *J. Am. Ceram. Soc.,* **64** [1] 19 (1981) 22

Chapter 5

Synthesis of Oxide Nanophosphors for Electroluminescent Lamp Applications

5.1 Introduction

Powder EL displays have virtually unlimited potential [1]. Especially flexible powder EL devices can be manufactured on flexible substrates such as a film of polyethylene terephthalate (PET) coated with indium tin oxide (ITO). On account of these features, powder EL devices are used to liquid crystal display (LCD) backlight such as cellular phones, personal digital assistant (PDA) and palmtop computer [2]. Powder EL lights can also be used for architectural and decorative lighting. However, the sulfide phosphors used for commercially available EL devices have hydroscopic characteristics and a short-term reliability. The biggest problem with the powder EL devices is the instability of sulphide phosphors or organic binder, and their short lifetime of 2500 h at 200 V and 400 Hz in comparison with general fluorescent lamp with lifetime of 10,000 h [2,3]. Thus, oxide phosphors are required to overcome these inferior characteristics. $ZnGa_2O_4/Mn^{2+}$ phosphor can satisfy the main requirement for long lifetime. Also this phosphor has been known for high efficiency in thin film EL and cathode-luminescence.

In this work, we have synthesized Mn^{2+} doped zinc gallate and zinc silicate phosphor. Slight indication of EL has been observed, the structural and optical properties have also been investigated.

5.2 Experimental Section

(a) Material Synthesis:

Oxide phosphors namely $ZnGa_2O_4$: Mn^{2+} (ZGO) and Zn_2SiO_4: Mn^{2+} (ZSO) phosphors were synthesized by a process discussed in section 2.1.3 and 2.1.4 respectively.

(b) Device Fabrication:

The MISIM structure for EL device was fabricated by taking a conducting glass (NESA) coated with Y_2O_3 . Figure 5.1 shows Y_2O_3 coated NESA used as substrate for the device. The roughness of the surface was measured by optical profiler under PSI mode keeping

magnification at 2.5 k. The measured roughness values for these two areas (a) and (b) are Ra = 54.53 nm; Rq= 65.08 nm; R_t= 1.17 nm and Ra =77.97 nm; Rq=104.30 nm; R_t= 839.36 nm respectively. These values and figure 5.1 indicate that surface (a) is more uniform than surface (b).

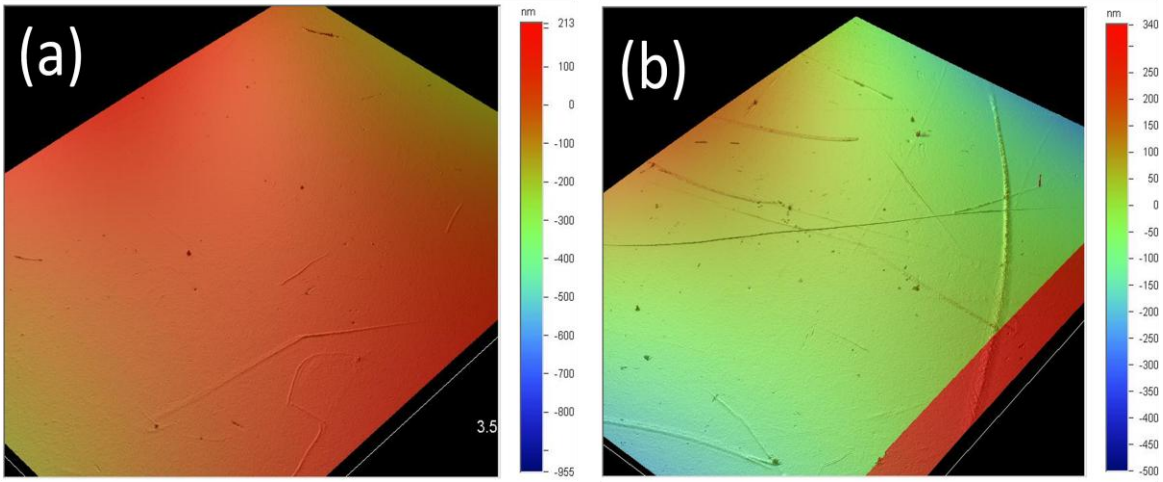

Figure 5.1: Images of Y_2O_3 Coated Optical profiler Figure

(c) Characterization:

The phase purity was checked by x-ray powder diffractometer of Bruker D-8 make with Cu Kα radiation operated at 35 kV and 30 mA. Microstructures of the nanocrystal samples were observed using scanning electron microscope (SEM, S-3700 Serial no. 370919-01) at DTU. The photoluminescence (PL) & Time resolved photoluminescence (TRPL) spectra were recorded using an Edinburgh Luminescence Spectrometer (Model: F900) fitted with a xenon lamp in the scan range from 200-800 nm at room temperature. UV-VIS-NIR spectrophotometer, the Hitachi model no. U-3900H was used for band gap measurements. The roughness of substrates was analysed by optical profiler (Veeco Wyko NT 9800). The dopant concentration studies were carried out using the Vario 6 Atomic Absorption Spectroscopy system from Analytikjena

5.3 Results and Discussion

(a) UV-VIS-NIR studies:

It is well known that the UV-VIS-NIR spectrum gives the information related to the band gap of the semiconductor. In the present case, band gap of $ZnGa_2O_4$: Mn^{2+} and $Zn_2SiO4:Mn^{2+}$ were determined from the absorbance spectrum recorded in the range 190 nm to 900 nm using UV-VIS-NIR spectrophotometer. Although, the absorption edge is indicative of the location of the band gap, accurate estimation of the band gap was determined by plotting $(\alpha h\nu)^2$ *vs.* $h\nu$, as shown in figure 5.2 . The band gap 'E_g' was identified as the intercept of the straight line thus obtained. Here α is the absorption coefficient and $h\nu$ is the energy of incident photons. The absorption coefficient (α) was determined by the relation $\alpha = A/t$, *t* being the optical path length of the light travelled through the sample and A measured absorbance. Optical path covered by the light was equal to 1 cm. Intersection of the tangent to the straight line and x-axis gave the band gap of the samples. Significant decrease in the band gap of the Zn_2SiO_4 samples as compared to $ZnSiO_3$ was observed which suggested increase in semiconducting property for Zn_2SiO_4 sample. Calculated value of the band gaps of $ZnGa_2O_4$:Mn and Zn_2SiO_3:Mn has been illustrated in Table 5.1.

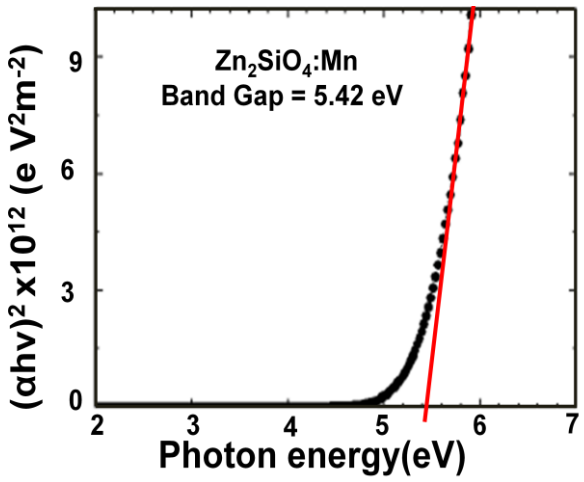

Figure 5.2: Band gap calculations for Mn doped zinc silicate using Tauc Method

Table 1.1: Band gaps of synthesized oxide phosphors

S.No.	Sample Name	Band Gap (eV)
1	$ZnGa_2O_4$:Mn	4.55
3	Zn_2SiO_3:Mn	5.42

(b) Scanning Electron Microscopy (SEM) observations:

In order to understand the surface morphology of ZGO and ZSO samples, electron microscopy observations have been performed. Figure 5.3 and 5.4 shows the SEM images for all the samples made using solid state reaction. It was found out that zinc gallate crystals were in the form of agglomerates with the particle size between 230 nm and 3.5 µm approximately. It is interesting to observe that ZSO made by SPS technique resulted in smaller particles sizes (variation between 760 nm and 0.6 µm). ZGO and ZSO particles both are almost spherical in shape but the size and shape distribution in ZSO particles is more uniform when compared with ZGO as depicted by figures 5.3 and 5.4.

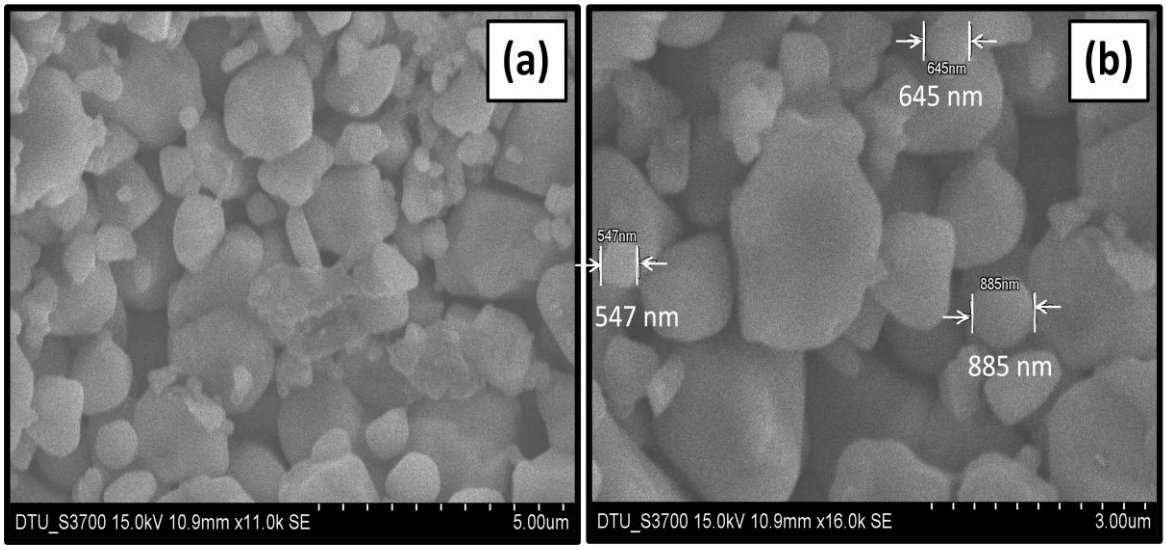

Figure 5.3: SEM Images of $ZnGa_2O_4$:Mn at 11 and 16 kX magnifications

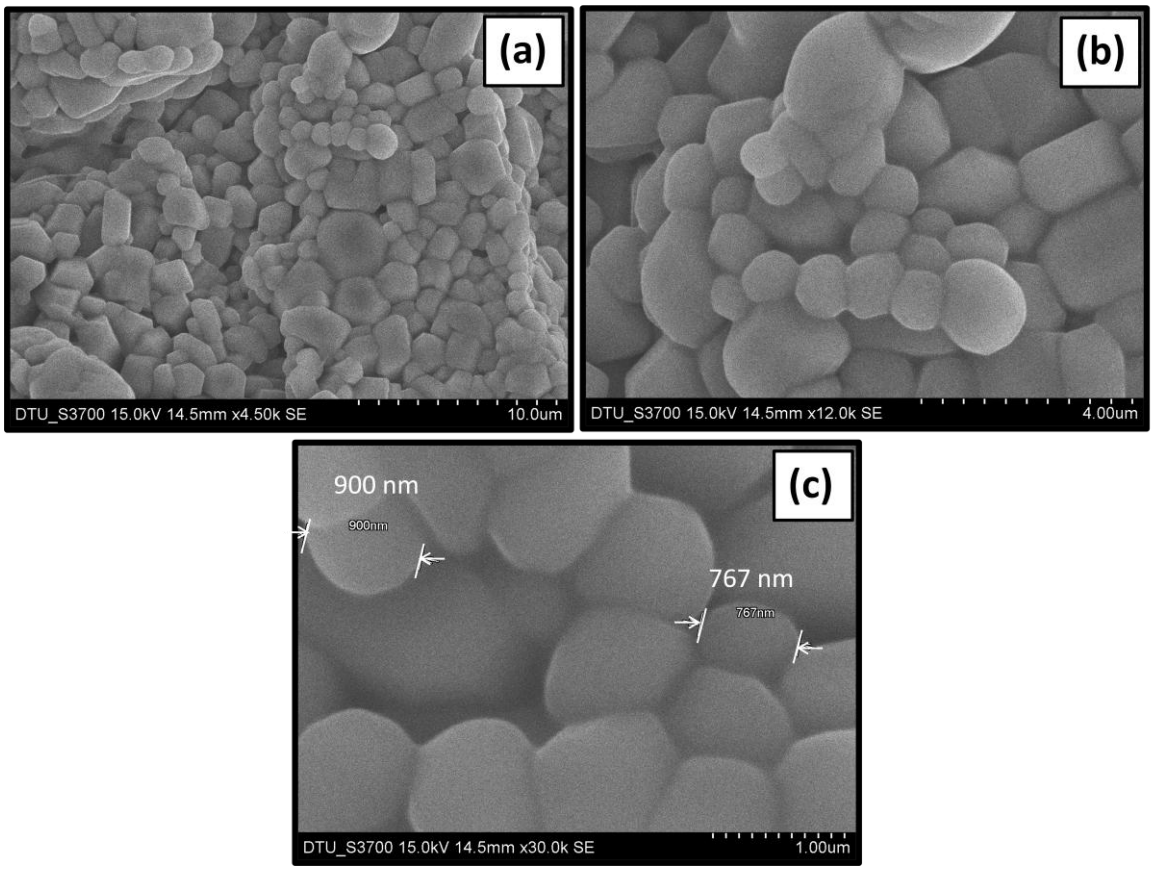

Figure 5.4: SEM images of Zn_2SiO_4: Mn at 4.5, 14.5 and 30 kX magnifications respectively

To know the elemental composition Energy Dispersive X-Ray spectroscopy was carried out. Table 5.2 show the EDAX studies of Zn_2SiO_4:Mn taken at voltage 15.0 kV keeping take off angle at 83.1 degree.

Table 5.2: Quantitative results for Mn doped zinc silicate

Element Line	Net Counts	Int. Cps/nA	Weight %	Weight % Error	Atom %	Atom % Error	Formula
O K	0	0.000	0.00	---	0.00	+/- 0.00	O
Si K	3	0.000	8.04	+/- 5.36	16.90	+/-11.27	Si
Si L	0	0.000	---	---	---	---	
Zn K	3	0.000	91.96	+/-122.62	83.10	+/-110.80	Zn
Zn L	1	0.000	---	---	---	---	
Total			100.00		100.00		

(c) Atomic Absorption Spectroscopy:

Atomic absorption spectroscopy (AAS) was carried out, in order to ascertain the amount of Mn^{2+} doping in the samples. Atomic absorption spectroscopy (AAS) is a spectro-analytical technique for the qualitative and quantitative determination of chemical elements present in the sample, employing the absorption of optical radiation (light) by free atoms in the gaseous state. In the current case, concentration of doped Mn^{2+} ions in zinc gallate and zinc silicate was estimated by AAS Vario 6 system from Analytikjena. It has been mentioned earlier that zinc gallate and zinc silicate samples were prepared by keeping the molar ratio of $Zn:Mn^{2+}$ as 1:0.001, 2:0.01, respectively. Since the doping was carried out using solid state reaction, it is possible that all the Mn^{2+} ions may not be doped into the $ZnGa_2O_4$ and Zn_2SiO_4 lattice and some of the un-reacted manganese ions may be present in the solution. The un-doped Mn^{2+} ions were removed by using glass fibre filter. This process was repeated thrice to ensure that all the un-reacted Mn^{2+} ions are removed. The actual concentration of doped Mn^{2+} estimated by AAS has been summarized in the table 5.3.

Table 5.3: Concentration of Mn^{2+} ions in ZGO and ZSO samples estimated by AAS

Sample	$Zn:Mn^{2+}$ Molar Ratio (Experimental)	Doped % of Mn^{2+} by AAS
$ZnGa_2O_4$	1:0.001	0.146%
Zn_2SiO_4	2:0.01	0.1784%

It is obvious from the AAS data that Mn^{2+} had been doped properly in oxide lattice and thus could contribute to commence luminescence.

(d) Powder X-ray diffraction (XRD) Analysis:

The phase identification of both the phosphor powders was carried out on with Cu-Kα radiation. Figure 5.5 shows X-ray diffraction patterns of $ZnGa_2O_4$: Mn powder. There are no ZnO-phase or Ga_2O_3-phase peaks discernible in ZGO sample. The sub solidus equilibrium study of the ZnO-Ga_2O_3 system showed no appreciable solid solubilities of ZnO or Ga_2O_3 in the $ZnGa_2O_4$ compound [4]. All the sintered powders exhibit the spinal structure of the $ZnGa_2O_4$ powder. The lattice constant of the $ZnGa_2O_4$: Mn powder was calculated to be 8.335 Å. The result is consistent with the value of 0.837 nm [5]. The concentration of Mn dopant is much less so that it cannot influence the crystal structure of host lattice.

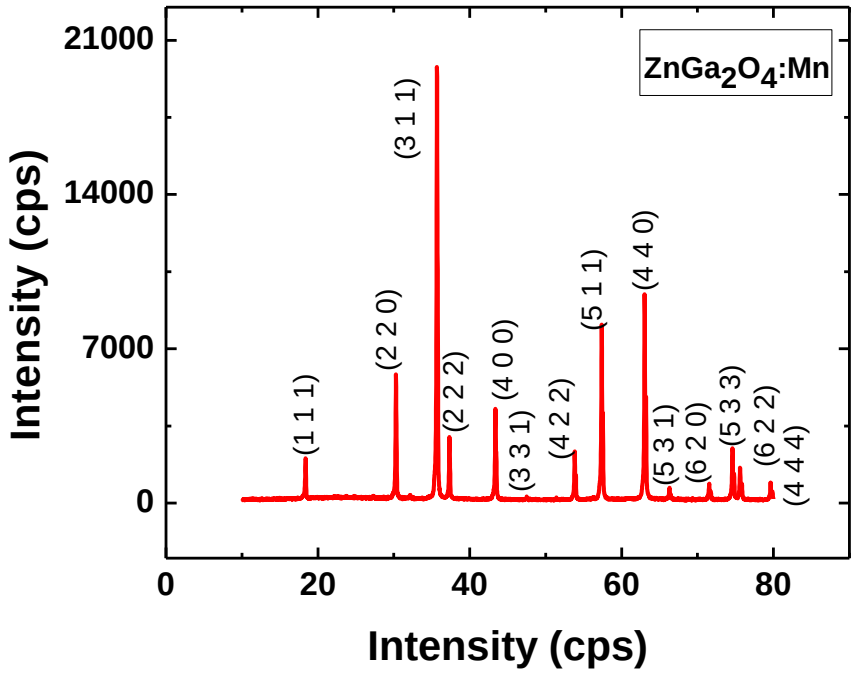

Figure 5.5: XRD of $ZnGa_2O_4$:Mn

Figure 5.6 shows the XRD spectra of the prepared Zn_2SiO_4: Mn powder. The diffraction pattern consists of peaks primarily associated with zinc silicate and no other spurious peaks were observed. The prepared sample doped with Mn^{2+} was found to match well with the reported data for rhombohedra willemite phase Zn_2SiO_4 (JCPDS 00-037-1485). The broadness of the diffraction peaks indicates that the material is in nano-regime.

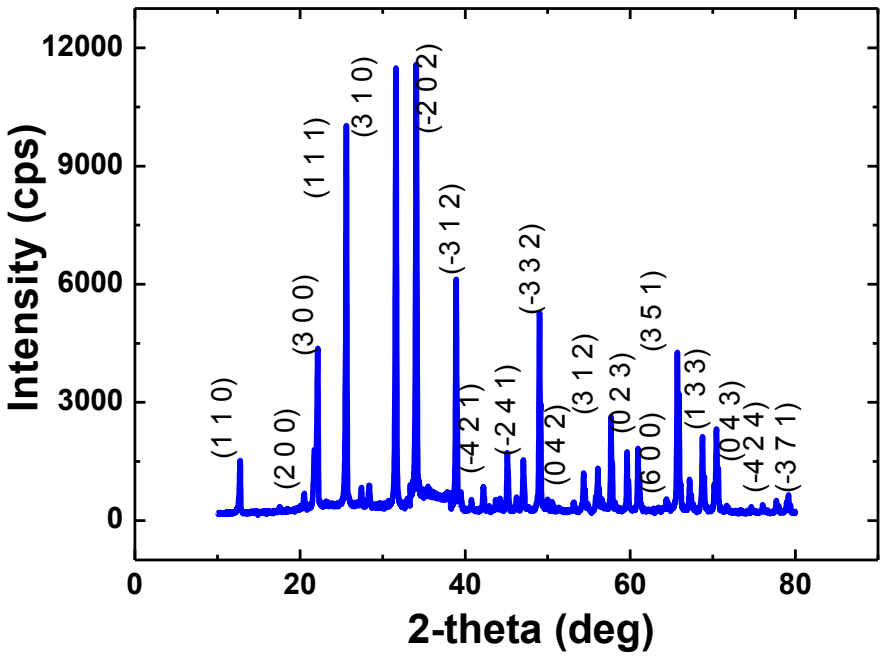

Figure 5.6: XRD of $ZnSi_2O_4$: Mn

(e) Photoluminescence Studies:

Photoluminescence spectroscopy is a contactless, non-destructive method of probing the electronic structure of materials. It gives the measure of the luminescence brightness and nature of luminescence. It consists of two parts, photoluminescence excitation (PLE) and photoluminescence emission (PL). PLE gives information about the absorbed energy which can excite the phosphor material to emit in the visible region. PL is the energy emitted by phosphor due to recombination of electron-hole pair. When the higher energy e.g. UV rays

fall on the sample, the emitted radiations from the sample are recorded on wavelength scale. The photoluminescence (PL) excitation and emission spectra for both the phosphors were collected at room temperature over the wavelength range from 200 to 700 with a resolution of 0.5 nm. The excitation source was a xenon discharge lamp.

Figure 5.7 presents the photoluminescence excitation and emission spectrum obtained from the annealed Zn_2SiO_4:Mn powder. The broad PL emission spectrum extends over a broad range of wavelengths from 490 to 610 nm with a peak maximum at around 520 nm in the green region. The full width at half maximum (FWHM) of the PL emission was measured to be approximately 35.31 nm. In the rhombohedra-crystal structured Zn_2SiO_4 host, the Mn^{2+} ion is incorporated substitutionally at the Zn^{2+} lattice site with tetrahedral site symmetry, forming the Mn_z^{2+} luminescent centre. The 3d orbital electrons in the Mn_z^{2+} ion relax radiatively from the $^4T_1$ (^4G) excited state to the $^6A_1$ (^6S) ground state, leading to the green PL emission [6].

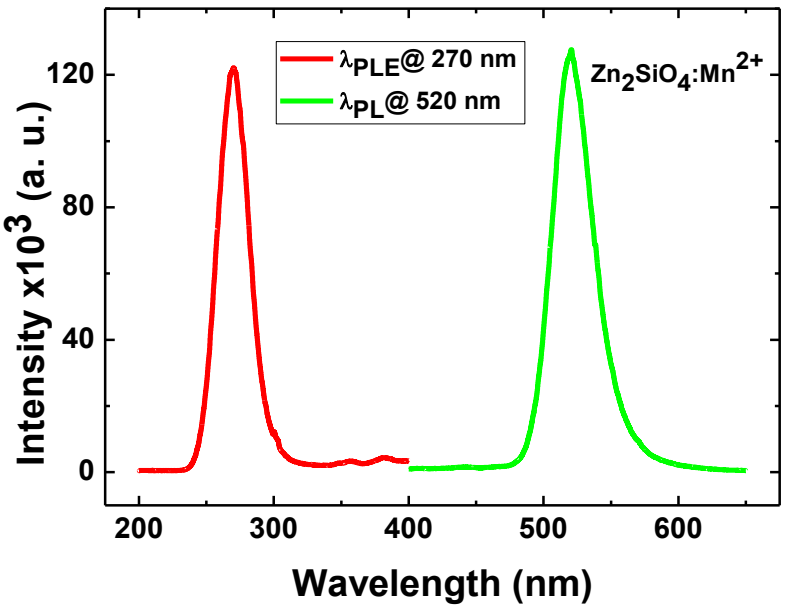

Figure 5.7: PL of Zn_2SiO_4:Mn^{2+} peaking at 520 nm on excitation with 270 nm

The observed PLE (excitation) spectrum showed a peak maximum at 270 nm with a FWHM of 27.163 nm, which was obtained at room temperature by monitoring the emission at a fixed wavelength of 520 nm. It can be seen from Fig. below that the threshold energy for excitation is approximately 4.35 eV. This threshold is considered to be the lowest energy required to excite the 3d orbital electrons in the Mn_z^{2+} ion from the $^6A_1$ (^6S) ground state to the conduction band (CB) of Zn_2SiO_4:Mn. The free electrons are, thus, generated in the conduction band by the charge transfer transition as described below:

$$Mn_z^{2+} (3d^5) \rightarrow Mn_z^{3+} (3d^4) + e_{CB}$$

These excited free electrons then relax from the conduction band to the $^4T_1(^4G)$ lowest excitation energy level of the Mn_z^{2+} ion through intermediate energy levels via non-radiative transitions, finally followed by a radiative transition from the $^4T_1(^4G)$ level to the $^6A_1(^6S)$ ground state. This results in the green PL emission peaking at 520 nm.

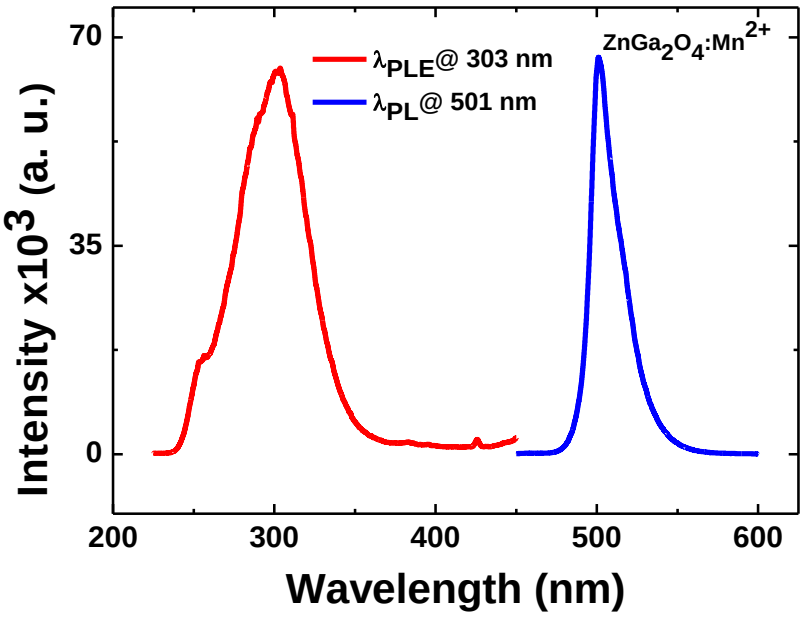

Figure 5.8: PL of ZnGa2O4: Mn peaking at 501 nm when excited with 303 nm

$ZnGa_2O_4$ is known to show green emission when it is doped with Mn^{2+} ions when excited by UV radiation peaking at 303 nm with Full width half maximum of 49.63 nm. The excitation energy of zinc gallate host is transferred in a non-radiative way from the Ga-O group in the host lattice to Mn^{2+} active centres, which results in green emission. The emission spectra of Mn doped $ZnGa_2O_4$ powder show a characteristic peak at 501 nm (Figure 5.8). The full width at half maximum (FWHM) of the PL emission was measured to be approximately 21.93 nm. The emission can be attributed to $^4T_1 \rightarrow {}^6A_1$transition of 3d electrons in the Mn^{2+} ion, which occupies the fourfold coordinated Zn position in the host material lattice. Figure 5.9 shows the photograph of $ZnGa_2O_4$: Mn showing green photoluminescence when seen under UV light of 350 nm.

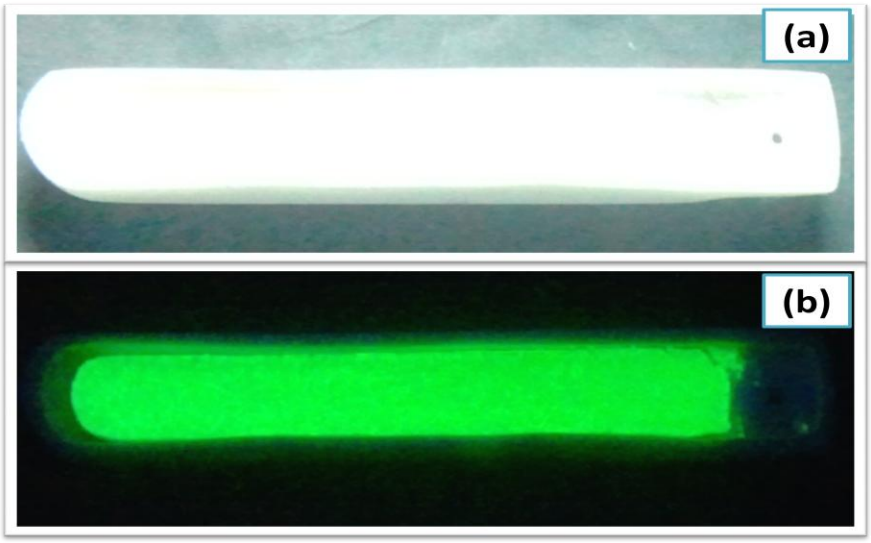

Figure 5.9: Mn^{2+} doped Zinc Gallate under (a) white light (b) UV light of wavelength 350 nm

The CIE coordinates of the PL emission of the $ZnGa_2O_4$ host, Mn doped samples and that of EL device are shown in figure 5.10. This clearly indicates the purity of the green colour of the Mn doped $ZnGa_2O_4$ oxide phosphor while the undoped powder samples shows blue emission. The purity of green colour of Mn doped $ZnGa_2O_4$ oxide phosphor depends on the Mn^{2+} concentration. The samples were annealed in a reducing atmosphere to convert the Mn^{4+} to Mn^{2+} to increase green emission intensity and to have good colour purity. The CIE colour coordinate are x = 0.0717; y = 0.6697 and for Zinc gallate and for zinc silicate these

values are x = 0.1958; y = 0.6996. These values are marked in the Standard CIE Graph as shown in figure 5.10.

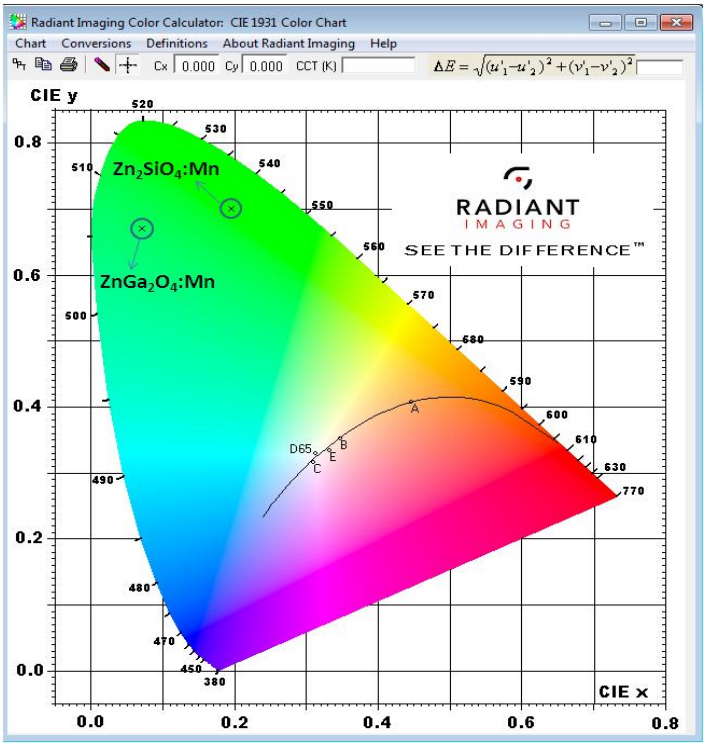

Figure 5.10: CIE colour coordinates of Mn^{2+} doped zinc gallate and zinc Silicate

(f) Time Resolved Photoluminescence Studies:

Time resolved PL (TRPL) spectroscopy is a non-destructive and powerful technique commonly used for measurement of free carrier or exciton lifetime, an important parameter related to material quality and device performance. The exciton lifetime varies with crystal sizes, becoming longer as the particle size increases. The efficiency of the radiative recombination is strongly related to the decay time of a particular transition. TRPL spectra

for oxide phosphors were obtained using Edinburgh luminescence spectrometer, model no. F-900 with nano second hydrogen and micro second flash lamps attachments and have been presented in figure 49 and 50. The variation in lifetime was calculated to be from millisecond (in the case Zinc silicate) to 30 minutes (in the case of zinc gallate). The TRPL decays for Zn_2SiO_4:Mn and $ZnGa_2O_4$:Mn were recorded at 519 nm emission and 270 nm excitation; and 501 nm emission and 303 nm excitation respectively, by a time correlated single photon counting technique. The luminescence lifetime in $ZnGa_2O_4$: Mn at 501 nm radiation was delayed for about 11.28 min. This indicates that, the smaller the size of particles, the shorter would be the luminescence lifetime.

The relative contribution (%) of each decay component was obtained by exponential fitting of the TRPL decay curves. The lifetime data and the parameters generated by the exponential fitting are listed in the inset of figure 5.11 and 5.12.

The lifetimes obtained for Zn_2SiO_4: Mn powder is 10.72 and 21.84 ms and that of zinc gallate are 11.28 and 20.94 min. respectively. The decay processes probably involve the radiative recombination of free electron–hole pairs as well as non-radiative charge transfer. The two decay components are as a result of the two distinct radiative events. First, the fast decay could be ascribed to the direct radiative transitions of the excitons from donor to acceptor level while the second, the slower component should be due to the radiative recombination via surface-trap sites. For longer lifetimes, one can easily attribute them to a donor–acceptor pair (DAP) type of recombination [7] usually observed for bulk materials.

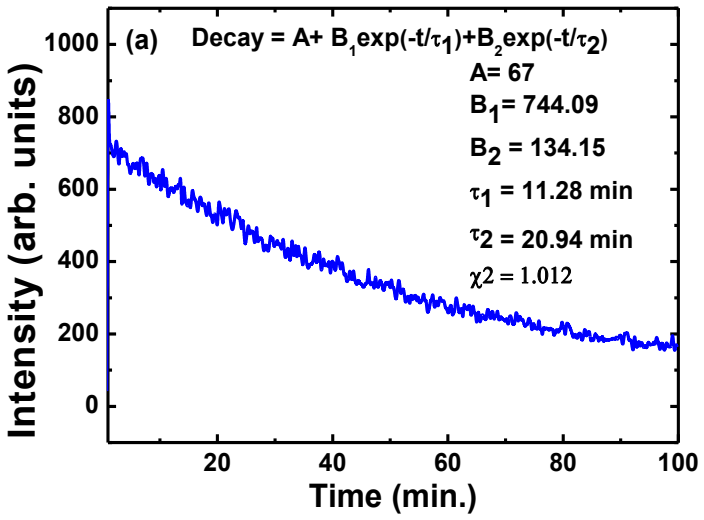

Figure 5.11: Time resolved photoluminescence after UV irradiation for $ZnGa_2O_4$:Mn (Excitation- 303 nm Emission at 501 nm)

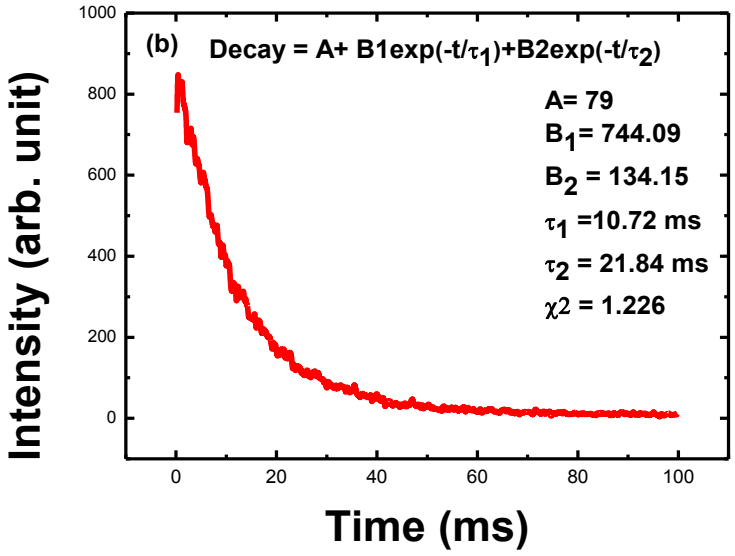

Figure 5.12 : Time Resolved Luminance after UV irradiation for Zn_2SiO_4:Mn (Excitation- 270 nm Emission at 519 nm)

5.4 Conclusions

Mn^{2+} doped zinc silicate and zinc gallate were prepared by solid state reaction method in inert atmosphere. The colour coordinates were calculated by equidistant wavelength method. The emission spectra for ZSO and ZGO were found to be peaking at 520 nm and 501 nm respectively. $^4T_1(^4G) \rightarrow {}^6A_1(^6S)$, is directly responsible for the green light emission. TRPL studies showed long time phosphorescence for ZGO sample. Bright electroluminescence was observed from both the phosphors (ZGO – 320 V_{AC}; 4 kHz and ZSO- 350 V; 5 kHz). These oxide phosphor based devices are chemically stable and have longer lifetime than that of the commercially available ZnS powder EL device.

References

[1] P.D. Rack, A. Naman, P.H. Holloway, S.S. Sun, R.T. Tuenge, MRS Bull. 21 (1996) 49.

[2] Y.A. Ono, Electroluminescent Displays, World Scientific, Singapore, 1995.

[3] S. Tanaka, J. Cryst. Growth 101 (1990) 958.

[4] C. W. W. Hoffmam and J. J. Brown Jr., J. Inorg. Nucl. Chem. 30 (1968) 63.

[5] T. Moeller and G. L. King, J. Am. Chem. Soc. 76 (1954) 6060.

[6] G. Blasse and B. C. Grabmaier, Luminescent Materials (Springer-Verlag, Berlin, Heidelberg (1994).

[7] L. Brus, J. Phys. Chem., 90 (1986) 2555.

Chapter 6

Conclusions and Scope for Future Work

Conclusions

Luminescence and basic concept associated with luminescence were learnt. In depth knowledge and skill was gained on various techniques for synthesizing nano-materials such as hydrothermal synthesis, solid state reaction, polyol synthesis, sol- gel synthesis, combustion method etc.

Properties of nanomaterial have been discussed. These materials have created a high interest in recent years by virtue of their unusual mechanical, electrical, optical and magnetic properties. Some examples are given below:

(a) Nanophase ceramics are of particular interest because they are more ductile at elevated temperatures as compared to the coarse-grained ceramics.

(b) Nanostructured metal-oxide thin films are receiving a growing attention for the realization of gas sensors (NOx, CO, CO_2, CH_4 and aromatic hydrocarbons) with enhanced sensitivity and selectivity. Nanostructured metal-oxide (MnO2) finds application for rechargeable batteries for cars or consumer goods. Nanocrystalline silicon films for highly transparent contacts in thin film solar cell and nano-structured titanium oxide porous films for its high transmission and significant surface area enhancement leading to strong absorption in dye sensitized solar cells.

(c) Polymer based composites with a high content of inorganic particles leading to a high dielectric constant are interesting materials for photonic band gap structure.

Apart from this we reported a high (~94%) yield synthesis of intrinsic zinc oxide (ZnO) nano-crystal powders having crystallite sizes in the range 13-35 nm using a novel gel-incineration method with inexpensive precursor salts and citric acid as chelating agent. The influence of various precursor chemicals on the nanocrystallite size, morphology and luminescent properties has been studied in detail. It was identified that the ZnO nanocrystals prepared using organic precursor resulted the smallest crystallite size as compared to inorganic precursors. Reaction temperature was optimized to be ~900°C by simultaneous thermogravimetric analysis and differential scanning calorimetry studies.

Morphology and microstructure of the ZnO nanocrystals have been studied using a scanning electron microscopy. Analysis of photoluminescence excitation and emission spectra enabled us to calculate the band gap energy and defect analysis of as prepared ZnO nanocrystals respectively.

We also developed powder electroluminescent materials using Mn^{2+} doped $ZnGa_2O_4$ and Zn_2SiO_4 phosphor with particle size of (~ 230 nm to 3.5μm). Band gap of zinc silicate was found to be 5.42 eV. Optical properties of powder electroluminescent device were investigated. ZGO and ZSO based devices emit green colour of 501 nm with a half width of 21.93 nm and 520 nm with a full width half maximum of 35.31 nm respectively. The origin of green colour is explained in terms of the energy transfer from warm carriers to Mn^{2+} centres via self-activated host centres. Long decay phosphorescence of ~30 minutes was observed in ZGO and is confirmed by time resolved photoluminescence studies.

Scope for Future Work

Nanomaterial formed by hydrothermal synthesis can be use in LED devices. Since formation of complex oxide is difficult at very low temperature. But with the help of this technique we can develop different type of structure. The synthesis technique is cost effective, one step and easy to control because it is performed at low temperature and normal atmospheric pressure.

Electroluminescent display technology is unique and relevant for today's embedded display solutions. The performance and visual characteristics of high-performance electroluminescent displays make it an ideal solution for the most challenging and demanding applications where other display technologies are simply inadequate. Electroluminescent displays are paper thin, flexible panels that can be produced to any size or shape and can be customised to either statically illuminate or animate to any sequence. Intensive research should be carried out to make this technology even better.

Highlights of the Research Work

We demonstrate a generic approach for the synthesis of single-crystal complex oxide nanostructures of various structure types using hydrothermal synthesis.

The method is based on a reaction between a metallic salt and a metallic oxide in a solution of composite-hydroxide eutectic at 185 °C and normal atmosphere without using an organic dispersant or capping agent.

The synthesis technique is cost-effective, one-step, easy to control, and is performed at low temperature and normal atmospheric pressure.

The technique can be expanded to many material systems, and it provides a general, simple, convenient, and innovative strategy for the synthesis of nanostructures of complex oxides with important scientific and technological applications in ferroelectricity, ferromagnetism, colossal magnetoresistance, fuel cell, optics, and more.

We also demonstrate a high (~94%) yield synthesis of intrinsic zinc oxide (ZnO) nanocrystal powders having crystallite sizes in the range 13-35 nm using organic and inorganic precursors. ZnO nanocrystals prepared using organic precursor resulted in the smallest crystallite size as compared to inorganic precursors. The stability of ZnO nanocrystals in water has been verified on time scale and its potential to be used as bio-medical applications.

What I learnt during the project work:

There was a lot to learn during the whole process, like how to survey the literature, finding a problem, what could be the possible solution to that, and how to optimize various parameters while solving it. I cultured to narrow down the things to reach to a specific result and how to analyze the things. I had great learning experiences while discussing the problems with the experts from the field.

"Instrument proficiency" gained / used in the project

1) Humidity and Temperature controlled Dry Box.
2) Microprocessor controlled High Temperature Furnace (Pyroton Make, India and MTI Corporation, USA) for Combustion synthesis and Solid state reaction.
3) High Pressure Vessel (Autoclave) from Parr Instruments Co., USA
4) Temperature Controlled Oven for autoclave heating.
5) Operation of Luminescence Spectrometers (Edinburgh F900 & Perkin Elmer LS-55)
6) Operation of UV lamp box having 254 nm, 285 nm and 370 nm emitting UV lights
7) Operation of centrifuge machine
8) Operation of temperature controlled ultrasonicator
9) Operation of Driving setup used for EL Devices
10) Operation of spin coating and dip coating units

Scientific output resulted from the Project

A. Research papers published in SCI Journals

1. *"High Yield Synthesis and Characterization of Aqueous Stable Zinc Oxide Nanocrystals Using Various Precursors"*

   G. Swati, Savvi Mishra, Deepika Yadav, R.K. Sharma, **Dileep Dwivedi**, N.Vijayan, J.S. Tawale, V. Shanker, D. Haranath

   Journal of Alloys and Compounds (Elsevier), 571 **(2013)** 1-5.

   [I.F.= 2.39]

B. Research papers communicated

1. *"Investigation of Local Field Enhancement and Hot Electron Injection in Carbon Nanotube Doped Phosphor Nanocomposites for Ultra-Bright Electroluminescence"*

   Deepika Yadav**,** **Dileep Dwivedi**, Savvi Mishra, B. Sivaiah, A. Dhar, V. Shanker and D. Haranath

   Composites Science and Technology (Under Review, June 2013)

   [I.F.=3.328]